The NDP52/CALCOCO2 selective autophagy receptor controls processing body disassembly

inflammatory cytokine transcripts / Kaposi's sarcoma-associated herpesvirus / NDP52 / processing bodies / selective autophagy

Carolyn-Ann Robinson[1,2,3,4], Gillian K. Singh[1,4], Elizabeth L. Castle[1], Bre Q. Boudreau[1], Jennifer A. Corcoran[1,2,3,5]

[1]Department of Microbiology & Immunology, Dalhousie University, Halifax, NS, Canada

[2]Microbiology, Immunology & Infectious Diseases Department, University of Calgary, Calgary, AB, Canada.

[3]Charbonneau Cancer Research Institute, University of Calgary, Calgary, AB, Canada.

[4]Equal Contribution

[5]Corresponding Author

Abstract

Processing bodies (PBs) are cytoplasmic ribonucleoprotein granules that control inflammation by silencing or degrading labile messenger RNAs (mRNAs) that encode inflammatory molecules. PBs often disassemble in response to virus infection, which correlates with increased synthesis of inflammatory proteins. We previously showed that the Kaposi's sarcoma-associated herpesvirus (KSHV) KapB protein causes PB disassembly. Here, we reveal that KapB-mediated PB disassembly depends on the canonical autophagy genes *Atg5* and *Atg14* or the selective autophagy receptor *NDP52/CALCOCO2*. Moreover, KapB expression increased inflammatory transcripts levels and this effect was also dependent on canonical autophagy and NDP52. Stimulating autophagy with the mTOR inhibitor Torin-1 also increased cytokine mRNA and required ATG5 and NDP52 to mediate PB disassembly. These studies reveal a new role for NDP52 in regulating inflammatory responses by promoting PB turnover and the concomitant synthesis of inflammatory molecules.

16 **Introduction**

17 Under basal conditions, autophagic activity ensures the continuous recycling of cellular
18 resources and the clearance of damaged macromolecular complexes and organelles, maintaining
19 cellular homeostasis and acting as an intracellular quality control system (Green *et al*, 2011;
20 Klionsky *et al*, 2012; Morishita & Mizushima, 2019; Levine *et al*, 2008). Various changes to the
21 cellular microenvironment, including nutrient scarcity, hypoxia, and endoplasmic reticulum (ER)
22 stress can drive autophagy and degradation of damaged organelles (e.g mitochondria,
23 peroxisomes), protein complexes (e.g. focal adhesion complexes), or other targets in a selective
24 manner (Maiuri & Kroemer, 2015; Mizushima *et al*, 2010; Balgi *et al*, 2009; Kenific *et al*, 2016;
25 Sargsyan *et al*, 2015; Tripathi *et al*, 2016; Dunn *et al*, 2005; Yao & Klionsky, 2016). In selective
26 autophagy, target cargo is selected for degradation either directly, by binding to lipidated
27 microtubule associated protein 1 light chain 3 (LC3) protein (LC3-II), or indirectly via molecular
28 bridges termed selective autophagy receptors (SARs). Some of the best characterized SARs
29 include p62/SQSTM1, valosin containing protein (VCP), optineurin (OPTN), neighbor of
30 BRCA1 gene 1 (NBR1), and nuclear dot protein 52 (NDP52/calcium binding and coiled-coil
31 domain protein, CALCOCO2) (Zaffagnini & Martens, 2016). OPTN, p62, NDP52, and NBR1
32 are members of the sequestosome-like family and contain several conserved motifs including a
33 LC3-interacting region (LIR) and a ubiquitin-binding domain (UBD) (Ichimura *et al*, 2008;
34 Noda *et al*, 2010; Birgisdottir *et al*, 2013; Noda *et al*, 2008). The selection of cargo for
35 degradation can occur in a ubiquitin-dependent or -independent manner, although ubiquitin
36 modification is believed to enhance cargo recruitment to autophagosomes (Rogov *et al*, 2014).
37 SARs play important homeostatic roles in maintaining, and at times magnifying, the turnover of
38 organelles and aggregates which facilitates cell survival in response to environmental changes

39 (Maiuri & Kroemer, 2015; Mizushima *et al*, 2010; Balgi *et al*, 2009; Kenific *et al*, 2016;
40 Sargsyan *et al*, 2015; Tripathi *et al*, 2016; Dunn *et al*, 2005; Yao & Klionsky, 2016).
41
42 SARs also play important roles in fine-tuning innate immune responses by targeting key
43 signaling platforms for degradation (Chen *et al*, 2016; Du *et al*, 2018; Jin *et al*, 2017; Prabakaran
44 *et al*, 2018; Yang *et al*, 2017; He *et al*, 2019). For example, NDP52 is required for the
45 autophagic degradation of interferon regulatory factor 3 (IRF3) and mitochondrial antiviral
46 signaling protein (MAVS), which supports the resolution phase of type I interferon signaling
47 (Wu *et al*, 2020) (Seth *et al*, 2005; Jin *et al*, 2017). Both pro and antiviral roles have been
48 attributed to SARs (Sumpter & Levine, 2011; Ahmad *et al*, 2018) and viruses can both enhance
49 or limit SAR function accordingly, promoting their replication (Mohamud *et al*, 2019).
50 Kaposi's sarcoma-associated herpesvirus (KSHV) is the infectious cause of two B-cell
51 malignancies and the endothelial cell cancer, Kaposi's sarcoma (KS), which is typified by
52 aberrant angiogenesis, tortuous leaky blood vessels, and inflammation (Cesarman *et al*, 1995;
53 Chang *et al*, 1994; Soulier *et al*, 1995). Infection with KSHV has two forms, a latent and a lytic
54 phase and it is the latent phase that predominates in KS tumours (Decker *et al*, 1996; Staskus *et*
55 *al*, 1997; Broussard & Damania, 2020). Like many viruses, KSHV manipulates the autophagic
56 machinery. During latency, the viral FLICE inhibitory protein (v-FLIP) binds Atg3 to suppress
57 the LC3 lipidation process during autophagosome biogenesis (Lee *et al*, 2009). KSHV also
58 expresses a viral cyclin D homolog (v-cyclin), that triggers DNA damage that that leads to
59 autophagy and cellular senescence (Leidal *et al*, 2012), facilitating the production and non-
60 conventional secretion of pro-inflammatory cytokines such as IL-1β, IL-6 and IL-8 (Young *et al*,
61 2009). Together, KSHV manipulation of autophagic flux prevents xenophagy, limits interferon

62 responses and enhances inflammatory cytokine production. Precisely how KSHV fine tunes
63 autophagy during latency to balance proviral and antiviral activities and promote chronic viral
64 infection is not clear.
65
66 Processing bodies (PBs) are ubiquitous, cytoplasmic, ribonucleoprotein (RNP) granules that
67 regulate expression of many cytokine RNA transcripts, making them important sites of
68 inflammatory control. PBs contain enzymes involved in mRNA turnover, including those that
69 mediate decapping (Dcp2; co-factors Dcp1a and Edc4/Hedls), 5'-3' exonucleolytic degradation
70 (5'-3' exonuclease Xrn1 and RNA helicase Rck/DDX6) and some components of the RNA-
71 induced silencing complex (Cougot *et al*, 2012; Hubstenberger *et al*, 2017; Corbet & Parker,
72 2019; Youn *et al*, 2018; Riggs *et al*, 2020; Mohamud *et al*, 2019; Luo *et al*, 2018). mRNAs are
73 routed to PBs for decay and/or repression by RNA-binding proteins (RBPs) through recognition
74 of common sequence elements (Hubstenberger *et al*, 2017). AU-rich elements (AREs) are
75 destablilizing RNA regulatory elements found in the 3' untranslated regions of ~8% of cellular
76 transcripts that are responsible for targeting RNAs to PBs (Barreau *et al*, 2005; Bakheet *et al*,
77 2018; García-Mauriño *et al*, 2017). When bound by destabilizing RBPs, ARE-containing RNAs
78 are directed to PBs and suppressed (Maitra *et al*, 2008; Lai *et al*, 1999; Lai & Blackshear, 2001).
79 Our group and others showed that microscopically visible PBs correlate with the constitutive
80 turnover or translational suppression of ARE-mRNAs; when PBs are dispersed, this suppression
81 is reversed (Corcoran *et al*, 2012, 2015; Franks & Lykke-Andersen, 2007; Blanco *et al*, 2014;
82 Vindry *et al*, 2017). Because ARE-mRNAs code for potent regulatory molecules such as
83 inflammatory cytokines, PBs are important post-transcriptional regulator that fine tune the
84 production of inflammatory cytokines whose transcripts contain AREs, including IL-6, IL-8, IL-

85 1β, and TNF (Ensoli *et al*, 2010; Ensoli & Stürzl, 1998; Lane *et al*, 2002; Miles *et al*, 1990; Riva
86 *et al*, 2010; Sadagopan *et al*, 2007; Salahuddin *et al*, 1988; Bakheet *et al*, 2018).
87
88 PBs are dynamic structures that are continuously assembled and disassembled, yet relatively
89 little is known about how they are regulated. Stimuli that activate the p38/MK2 MAP kinase
90 pathway as well as many virus infections elicit PB disassembly and a concomitant reduction in
91 ARE-mRNA suppression to promote inflammatory molecule production (Corcoran *et al*, 2012,
92 2015; Vindry *et al*, 2017; Corcoran & McCormick, 2015; Standart & Weil, 2018; Docena *et al*,
93 2010). We have previously shown that KSHV causes PB disassembly during latent infection, and
94 that the viral protein Kaposin B (KapB) induces PB disassembly while enhancing the production
95 of an ARE-containing reporter (Corcoran *et al*, 2015; Corcoran & McCormick, 2015; Corcoran
96 *et al*, 2011). These data support the notion that PB disassembly is likely an important contributor
97 to inflammation associated with KS (Corcoran *et al*, 2015; Wen & Damania, 2010). Although we
98 know that KapB binds and activates the kinase MK2, and that MK2 is an important component
99 of the mechanism of KapB-mediated PB disassembly and ARE-mRNA stabilization, we do not
100 precisely understand how PB loss is elicited by KapB (McCormick & Ganem, 2005; Corcoran *et*
101 *al*, 2015). The observation that MK2 can phosphorylate Beclin-1 to increase autophagic flux in
102 response to nutrient scarcity (Wei *et al*, 2015) suggested to us that KapB may also drive
103 autophagic flux. We now show that the KSHV KapB protein enhances autophagic flux, revealing
104 an additional layer of complexity in viral regulation of autophagy during KSHV latency. We also
105 show that KapB requires canonical autophagy machinery Atg5 and Atg14 to induce PB
106 disassembly and ARE-mRNA stabilization and that KapB selects PB components for autophagic
107 turnover using the selective autophagy receptor, NDP52. PB turnover is also elicited by the

108 mTOR inhibitor and potent autophagy inducer, Torin-1, and this process is also dependent on
109 Atg5 and NDP52. In contrast, and despite previous observations that it elicits PB disassembly
110 and ARE-mRNA stabilization (Corcoran *et al*, 2015), a constitutively active form of MK2 does
111 not rely on canonical or selective autophagy machinery for PB loss. Our data reveal that cells
112 possess both autophagy-dependent and -independent mechanisms to regulate PB turnover and
113 inflammatory molecule production. These data also forge a new connection between the
114 selective autophagy receptor, NDP52, and cytoplasmic PBs, both of which control innate
115 immune responses and inflammation.
116

117 **Results**

118 **KapB induces autophagic flux**

119 KapB expression activates the stress-responsive kinase MAPKAPK2 (MK2) (McCormick &
120 Ganem, 2005; Corcoran *et al*, 2015). Since MK2 phosphorylates the essential autophagy inducer
121 Beclin 1 in response to amino acid starvation (Wei *et al*, 2015; Shen *et al*, 2016; Gurkar *et al*,
122 2013), we questioned whether KapB expression could promote autophagic flux. Essential for
123 autophagosome expansion is the lipidation of LC3 to form LC3-II, permitting its incorporation
124 into autophagosome membranes (Klionsky *et al*, 2012). To measure autophagic flux, we
125 examined levels of LC3-II and the SAR, p62, with and without treatment with the lysosomal
126 inhibitor, Bafilomycin A1 (BafA1), as both LC3-II and p62 are also substrates for autophagy
127 (Mizushima *et al*, 2010; Mauvezin & Neufeld, 2015). To this end, human umbilical vein
128 endothelial cells (HUVECs) were transduced with lentiviral vectors that express KapB or an
129 empty vector control and treated for increasing times with BafA1; LC3-II and p62 accumulation
130 in the presence or absence of BafA1 treatment was determined by immunoblotting. When KapB-
131 expressing cells were treated for 4 h with BafA1, the amount of LC3-II and p62 increased two-
132 and four-fold, respectively, compared to untreated cells. Both proteins showed higher
133 accumulation after BafA1 treatment of KapB-expressing cells than equivalently treated vector
134 controls (Fig 1A), indicating that autophagic flux was specifically enhanced in KapB-expressing
135 cells. We also measured endogenous LC3 puncta using immunofluorescence as an indicator of
136 autophagic flux (Kabeya, 2000; Mizushima *et al*, 2010). Untreated KapB-expressing HUVECs
137 displayed LC3 puncta area similar to that of control cells; however, LC3 puncta area increased
138 after BafA1 treatment, further suggesting that KapB expression enhanced autophagic flux (Fig
139 1B). Taken together, these data show that KapB expression induced autophagic flux in HUVECs.

140 **Canonical autophagy is required for KapB- and Torin-mediated PB disassembly**

141 Our group previously described that MK2 activation was an important component of KapB-
142 mediated PB loss (Corcoran *et al*, 2015); however, these experiments did not reveal the precise
143 mechanism of PB loss nor did they clarify if KapB was causing PB disassembly or blocking PB
144 assembly. Since PBs are dynamic RNP granules, we wanted to determine whether KapB-
145 mediated PB loss was a result of enhanced disassembly of PBs or prevention of their *de novo*
146 assembly. To do so, we utilized HeLa cells that express a Dox-inducible GFP-tagged version of
147 the PB-resident protein, Dcp1a (Youn *et al*, 2018). When fixed, GFP-positive puncta co-stain
148 with endogenous PB proteins such as the RNA helicase DDX6/Rck and the decapping co-factor
149 Hedls/Edc4, indicating that they represent PBs (Fig S1). KapB was transfected into these cells
150 either before or after inducing GFP-Dcp1a granule formation. When KapB was expressed prior
151 to granule induction, Dcp1a puncta formation was intact, although their appearance was slightly
152 delayed compared to vector control cells (Fig S1A). However, when KapB was expressed after
153 granule induction, GFP-positive puncta were lost (Fig S1B), indicating that KapB expression
154 induced PB disassembly. As further evidence, we treated KapB-expressing HUVECs with
155 sodium arsenite, a known inducer of PB assembly. We observed that sodium arsenite induced
156 endogenous PB formation in KapB-expressing HUVECs that was indistinguishable from
157 equivalently treated control cells (Fig S1C). Taken together, these results show that KapB
158 expression caused PB loss by inducing PB disassembly but did not block PB assembly. We
159 speculated that KapB may be utilizing a normal cellular pathway that mediates the turnover of
160 RNPs, such as autophagy.

161 To determine if autophagy was required for KapB-mediated PB disassembly, we first inhibited
162 autophagic flux by independently silencing two canonical autophagy genes, Atg5 and Atg14 (Fig

163 S2A, B). When either Atg5 or Atg14 were silenced in KapB-expressing HUVECs, PBs were
164 restored, whereas their silencing did not have an effect in control cells (Fig 1C and D). We then
165 examined the ability of KapB to mediate PB disassembly in Atg5 -/- MEFs, which are defective
166 for autophagy (Katayama *et al*, 2008), as indicated by the lack of LC3-II (Fig S2C). KapB failed
167 to disassemble PBs in Atg5 -/- MEFs but did disassemble PBs in matched wild-type controls
168 (Fig S2D). Moreover, KapB expression resulted in a significant increase in Atg5 protein levels
169 (Fig S2A), consistent with our other data that show that KapB is promoting autophagy. Blocking
170 autophagic degradation with BafA1 also restored PBs in KapB-expressing cells (Fig 1E). These
171 data suggest that KapB is accelerating PB turnover by enhancing autophagy.

172 Autophagy, although always occurring at a basal level, can be upregulated by many different cell
173 stimuli including starvation or inhibition of mTOR using Torin-1, hereafter referred to as Torin
174 (Thoreen *et al*, 2009). It was previously reported that rapamycin, an inhibitor of mTORC1,
175 caused a loss of PBs in mammary epithelial cells (Hardy *et al*, 2017). We reasoned that if we
176 inhibited both mTOR complexes mTORC1 and mTORC2 (Liu *et al*, 2013) using Torin, PBs
177 would disassemble. We observed that the number of Hedls/Edc4 puncta were significantly
178 reduced after Torin treatment, indicating that chemical induction of autophagy also resulted in
179 the disassembly of PBs in HUVECs (Fig 2A). To ensure that Torin treatment was inducing
180 disassembly of PBs and not preventing assembly, HUVECs were treated with sodium arsenite to
181 induce PB formation; like KapB, Torin treatment did not prevent the assembly of PBs under
182 stress conditions (Fig 2B). We then silenced Atg5 and tested if Torin treatment was able to
183 disassemble PBs in these cells. Although Torin caused PB disassembly in control cells, Torin
184 failed to alter the number of Hedls/Edc4 puncta in cells expressing shAtg5 (Fig 2C). Taken

185 together, these data show that PB turnover requires autophagy in response to both KapB and
186 Torin.

187 **Canonical autophagy is required for KapB-mediated increases in ARE-containing cytokine**
188 **transcripts**

189 PBs are nodes of mRNA regulation and microscopically visible PBs are associated with ARE-
190 mRNA decay or suppression (Guo *et al*, 2018; Luo *et al*, 2018; Corcoran *et al*, 2015, 2012;
191 Franks & Lykke-Andersen, 2008; Vindry *et al*, 2017; Blanco *et al*, 2014). We treated HUVECs
192 with conditioned media from latent KSHV-infected cells to stimulate the transcription of
193 inflammatory RNAs in a biologically relevant manner and examined levels of some endogenous
194 ARE-containing RNA transcripts in KapB-expressing cells (Fig 3A). We observed significant
195 increases of cytokine mRNA for IL-6 and IL-1β in KapB-expressing cells compared to
196 equivalently treated controls, suggesting these increases resulted from reduced transcript
197 turnover in PBs (Fig 3A). In addition, treatment with Torin promoted the enhanced steady-state
198 levels of IL-1β and COX-2 (Fig 3B), suggesting that inducing autophagy reduces turnover of
199 some ARE-mRNA transcripts. To support these findings and to simplify further studies, we
200 utilized a luciferase reporter assay that we previously developed, described in (Corcoran *et al*,
201 2011). We previously used this assay to show that KapB-mediated PB loss correlated with
202 enhanced luminescence of an ARE-containing firefly luciferase (Fluc) reporter because its rapid
203 turnover was reversed and FLuc translation was enhanced (Corcoran *et al*, 2011, 2015). Briefly,
204 HeLa cells were co-transfected with a FLuc construct containing the AU-rich element from
205 CSF2 in its 3'UTR and a Renilla luciferase (RLuc) construct with no ARE; transcription of both
206 reporter constructs was then stopped by the addition of doxycycline. In control (vector
207 transfected) cells, the FLuc-ARE mRNA decayed rapidly and FLuc luminescence relative to the

208 RLuc transfection control was low. Torin treatment caused a significant increase in FLuc/RLuc
209 relative luminescence compared to DMSO-treated control cells, supporting our RT-qPCR
210 findings (Fig 3C) and suggesting that enhanced autophagy reverses the constitutive
211 turnover/suppression of the ARE-mRNA reporter. Furthermore, KapB expression also caused a
212 significant increase in FLuc/RLuc relative luminescence compared to empty vector control cells
213 (Fig 3D) as previously shown in (Corcoran *et al*, 2015). When canonical autophagy was
214 perturbed by either Atg5 or Atg14 silencing (Fig S3A, B) KapB-expressing cells had
215 significantly decreased luminescence compared to KapB-expressing controls (Fig 3D, E).
216 Likewise, when KapB-expressing cells were treated with BafA1, relative luminescence was
217 significantly decreased compared to KapB-expressing untreated control cells (Fig 3F). Together,
218 these data showed that canonical autophagy is required for KapB-mediated increases in cytokine
219 mRNA levels and the enhanced expression of an ARE-mRNA reporter.
220

221 **Dcp1a protein levels are decreased by KapB and Torin treatment**

222 We reasoned that if KapB and Torin required autophagy for PB turnover, KapB expression or
223 Torin treatment may decrease steady-state levels of one or more key PB proteins that have
224 important scaffolding roles for granule formation, such as EDC4/Hedls, Xrn1, DDX6/Rck, or
225 Dcp1a (Ayache *et al*, 2015). Immunoblotting for these proteins revealed that steady-state levels
226 of the PB-resident protein Dcp1a were reduced in Torin-treated (Fig 4A) and KapB-expressing
227 cells (Fig 4B); however, steady-state levels of other PB-resident proteins were not affected (Fig
228 4A, C). These data suggest that autophagy induction with Torin or KapB expression promote the
229 turnover of the PB-resident protein Dcp1a, but not all PB proteins. Silencing the canonical

230 autophagy gene, Atg5, resulted in a reversal of KapB-mediated Dcp1a loss (Fig 4D), suggesting
231 that autophagy is required for the loss of Dcp1a observed after KapB expression.

232

233 **KapB-mediated PB disassembly and ARE-mRNA stabilization require the selective**
234 **autophagy receptor NDP52**

235 After establishing a link between KapB expression, autophagy, and PB disassembly, we
236 wondered what specific autophagy mechanisms were at work and if selective autophagy
237 receptors (SARs) were involved. Very little is known about how PB dynamics are regulated;
238 however, one previous study observed the SAR, NDP52, partially co-localized with some PB
239 proteins (Guo *et al*, 2014). For this reason, we investigated whether NDP52, p62, VCP, NBR1,
240 or OPTN were required for KapB-mediated PB disassembly using RNA silencing. Despite trying
241 several different shRNA sequences, our attempts to silence NBR1 were unsuccessful, and
242 shRNAs targeting VCP resulted in significant HUVEC toxicity (Fig S4A, B). Therefore, the role
243 of these molecules in PB turnover could not be determined in our model. Genetic knockdown of
244 NDP52, p62, and OPTN was validated in control and KapB-expressing cells (Fig S4C-E). In
245 these experiments, silencing of p62 or OPTN did not restore PBs in KapB-expressing cells
246 whereas NDP52 knockdown significantly restored PBs (Fig 5A, Fig S4F). These data pinpointed
247 an important role for NDP52 and selective autophagy in KapB-mediated PB disassembly. We
248 then tested whether NDP52 silencing could prevent Torin-mediated PB disassembly and found
249 that PBs could not be disassembled in cells lacking NDP52 (Fig 5B, S4G). We also examined
250 whether these SARs were required for KapB-enhanced relative luminescence in our ARE-
251 mRNA reporter assay. We validated silencing of NDP52, p62, and OPTN in HeLas (Fig S5A-C).
252 Similarly, we found that p62 or OPTN knockdown had no effect on KapB-mediated FLuc/RLuc

253 luminescence, but NDP52 silencing decreased FLuc/RLuc luminescence compared to non-
254 targeting, KapB-expressing controls (Fig 5C), further supporting the role of NDP52 in
255 autophagy-mediated PB disassembly. Therefore, KapB-stimulated PB disassembly and
256 concomitant luminescence of our ARE-containing reporter uses a mechanism dependent on
257 NDP52.

258 **NDP52 requires the ubiquitin-binding domain for KapB-mediated PB disassembly**

259 NDP52 has many functions in selective autophagy and autophagosome maturation and is a
260 crucial adaptor for mitophagy and xenophagy (Ellinghaus *et al*, 2013; Fu *et al*, 2018; Lazarou *et*
261 *al*, 2015; Morriswood *et al*, 2007; Verlhac *et al*, 2015). Structural domains that are important for
262 the function of NDP52 as a SAR include a non-canonical LC3-C interacting region (cLIR) that
263 binds to LC3-decorated autophagosomes and a ubiquitin binding domain (UBD) that binds
264 ubiquitinated cargo proteins, linking them to the autophagosome for engulfment (Fig 5D)
265 To elucidate if NDP52 was required for KapB-mediated PB disassembly because of its ability to
266 promote selective autophagy, we performed a complementation experiment. We first silenced
267 endogenous NDP52 in control or KapB-expressing HUVECs using shRNAs targeting the 3'UTR
268 of NDP52 and verified its knockdown (Fig S6A). Next, NDP52 expression was restored by
269 overexpressing a fluorescently tagged NDP52 construct. Complementation of NDP52-silenced
270 HUVECs with wild-type NDP52 restored KapB-mediated PB disassembly compared to vector
271 controls (Fig 5E, F; S6B, C). We next sought to determine whether the PB disassembly initiated
272 in KapB-expressing cells was reliant on two domains of NDP52 that are important for its role as
273 a SAR: the LIR and UBD. We restored NDP52 expression in NDP52-silenced HUVECs by
274 complementation with a fluorescently tagged UBD mutant (C443K) or a cLIR and UBD
275 combined mutant (V136S and C443K) (Padman *et al*, 2019; Ellinghaus *et al*, 2013; Till *et al*,

276 2013) (Fig 5E, F). Complementation with either of the mutated forms of NDP52 failed to restore
277 KapB-mediated PB disassembly in NDP52-silenced HUVECs. These data indicated that the
278 UBD of NDP52 is required for KapB-mediated PB disassembly and suggest that the LIR domain
279 may also be important (Fig 5E, F). These data provide evidence to support that the function of
280 NDP52 in selective autophagy is required for its role in KapB-mediated PB disassembly.
281

282 **Canonical autophagy is not required for MK2-mediated PB disassembly**

283 Because we know that KapB can directly bind and activate MK2 (McCormick & Ganem, 2005)
284 and that MK2 is, in part, required for KapB-mediated effects on PBs and ARE-mRNA (Corcoran
285 *et al*, 2015), we reasoned that a constitutively active version of MK2 would also induce PB
286 disassembly in an autophagy-dependent manner. To test this, we used a phosphomimetic
287 construct called MK2EE in which two threonine residues that are normally phosphorylated by
288 p38 MAPK in response to stress signaling are substituted with glutamic acid residues, rendering
289 the kinase constitutively active (Kayyali *et al*, 2002; Rousseau *et al*, 1997). We previously
290 demonstrated that MK2EE causes PB disassembly (Corcoran *et al*, 2015) and others have shown
291 that it can also increase autophagic flux (Wei *et al*, 2015). We confirmed that autophagy was
292 upregulated in MK2EE-expressing HUVECs by staining for endogenous LC3 puncta. We
293 observed that BafA1 treatment resulted in a significant increase in LC3-puncta compared to
294 vector controls, consistent with enhanced autophagic flux (Fig 6A). Furthermore, MK2EE
295 expression resulted in an increased accumulation of LC3-II and p62 after Baf A1 treatment to
296 block degradation (Fig 6B). We then tested if MK2EE-induced PB disassembly was reliant on
297 autophagic flux. MK2EE-expressing HUVECs retained the ability to disassemble PBs after Atg5
298 silencing (Fig 6C, S7A). MK2EE expression was previously shown to increase the FLuc/RLuc

299 relative luminescence in our reporter assay (Corcoran *et al*, 2015) and we reproduced these data
300 herein (Fig 6D). However, Atg5 silencing did not significantly decrease MK2EE-mediated
301 relative luminescence (Fig 6D, S7B). These data suggest that although MK2EE induces
302 autophagy and PB disassembly, these are unrelated phenotypes and the manner by which
303 MK2EE induces PB loss does not require canonical autophagy pathways involving Atg5.

304 Given that MK2 induces autophagy, but MK2EE-mediated PB disassembly did not require
305 canonical autophagy machinery, we speculated that MK2EE-mediated PB disassembly could be
306 facilitated by NDP52. However, p62, NDP52 and OPTN silencing did not inhibit PB
307 disassembly in MK2EE-expressing cells (Fig S7C-E; 6E; S7F). Likewise, silencing of p62,
308 OPTN, or NDP52 did not decrease FLuc/RLuc luminescence in MK2EE-expressing cells as it
309 did in KapB-expressing cells (Fig 6F, S7G-I). In fact, NDP52 knockdown increased ARE-
310 mRNA stability (Fig 6F), although the significance of this observation is unclear. These data
311 confirm that MK2-mediated PB disassembly and enhanced ARE-containing luciferase reporter
312 expression do not require canonical autophagy or selective autophagy machinery.

313

314

315 **Discussion**

316 Here we demonstrate that the KSHV protein, KapB, relies on selective autophagy to cause PB
317 disassembly and enhance ARE-mRNA stability. We furthermore identified NDP52 as the
318 selective autophagy receptor required for this process. To our knowledge, this is the first report
319 that NDP52 regulates the turnover of endogenous PBs and the first description of the
320 contribution of NDP52 to immune regulation by altering inflammatory cytokine RNA
321 turnover/suppression in PBs. Our major findings are: i) KapB increases autophagic flux, thereby
322 contributing to the complex regulation of autophagic processes during KSHV latent infection and
323 tumourigenesis, ii) KapB-mediated PB disassembly and enhanced translation of an ARE-
324 containing reporter requires canonical autophagy machinery and the selective autophagy
325 receptor, NDP52, iii) Activation of autophagy by chemical inhibition of mTORC1 using Torin
326 causes PB disassembly using a mechanism that is dependent on canonical autophagy and
327 NDP52, suggesting that KapB manipulates an existing cellular pathway that regulates PB
328 catabolism, and iv) the mechanism of KapB- or Torin-mediated PB disassembly differs from that
329 induced by the constitutively active kinase, MK2 (MK2EE), which is autophagy- and NDP52-
330 independent. These results reveal that PB turnover is mediated by autophagy-dependent and -
331 independent mechanisms and shows that the viral KapB protein hijacks a host pathway that uses
332 NDP52 to enhance PB catabolism and promote inflammatory molecule production.

333

334 MK2 activation promotes autophagy by phosphorylating Beclin 1 (Wei *et al*, 2015); therefore,
335 we hypothesized that KapB, an MK2-activating viral protein (McCormick & Ganem, 2005),
336 would utilize autophagy to promote PB clearance. Our data showed that although both KapB and
337 MK2EE increased autophagic flux (Fig 1, Fig 6), only KapB-mediated PB disassembly required

338 the canonical autophagy proteins Atg5 and Atg14, and the selective autophagy protein NDP52
339 (Fig 1, Fig 5). MK2EE does not use an autophagy-dependent mechanism, as KapB does, for PB
340 disassembly and our studies have not yet revealed a mechanism for PB loss in these cells. These
341 data imply that cells employ more than one pathway to disassemble PBs, consistent with the dual
342 mechanisms responsible for turnover of other RNP granules like stress granules (Buchan *et al*,
343 2013; Turakhiya *et al*, 2018). Our data also suggest that KapB hijacks both these pathways to
344 utilize an MK2-dependent, autophagy-independent pathway and an NDP52-, autophagy-
345 dependent pathway to disassemble PBs, suggesting the central importance of PB loss to KSHV
346 latency. Our data are supported by previous work showing that in yeast, PB recycling requires
347 canonical autophagy machinery, and in mammalian cells NDP52 colocalizes with a GFP-tagged
348 version of Dcp1a when overexpressed (Buchan *et al*, 2013; Guo *et al*, 2014). We add
349 significantly to these studies, by performing our work in primary human endothelial cells and by
350 staining for endogenous PBs using immunofluorescence for the decapping co-factor
351 Hedls/EDC4. We reveal that when KapB is expressed, endogenous PBs are disassembled by an
352 Atg5-, Atg14-, and NDP52-dependent autophagy process. We also complemented NDP52-
353 silenced cells with an shRNA-resistant NDP52. We observed the restoration of KapB-mediated
354 PB disassembly when complementation was performed with wild-type NDP52 but not when
355 lacking the UBD (Fig 5). These data suggest that it is the ability of NDP52 to bind ubiquitinated
356 cargo for autophagic degradation that is required for KapB-mediated PB turnover, as has been
357 observed in other studies on NDP52 SAR function (Xie *et al*, 2015; Cemma *et al*, 2011).
358
359 Immunoelectron microscopy showed that PBs range in size from 150 to 350 nm and possess an
360 external area of peripheral protrusions that contain the helicase Rck/DDX6 anchored to a dense

361 central core of decay enzymes, including Dcp1a and Xrn1 (Cougot *et al*, 2012). Many PB-
362 localized enzymes are required for PB stability including Dcp1a; however, only three PB
363 proteins are required for *de novo* PB formation, DDX6, the translation suppressor, 4E-T, and
364 LSM14a (Ayache *et al*, 2015). Our data showed that KapB expression decreased the steady-state
365 levels of Dcp1a, while the steady-state levels of other PB proteins were unaffected (Fig 4).
366 Inducing autophagy with the mTORC1/2 inhibitor Torin recapitulated this effect, decreasing
367 steady-state levels of Dcp1a, but not other PB proteins (Fig 4). These data support a model where
368 the entire PB granule is not degraded by autophagy, but PB disassembly is induced by the
369 selective targeting of Dcp1a or another unidentified PB protein. Consistent with this, we show
370 that PBs can still form during KapB expression if we overexpress Dcp1a-GFP or block
371 translation using sodium arsenite (Fig S1). Dcp1a is also a target for other viruses that mediate
372 PB disassembly; for example, infection with poliovirus also caused PB disassembly and the loss
373 of Dcp1a over a time course of infection (Dougherty *et al*, 2011).
374
375 We do not yet understand how KapB expression or Torin treatment alters Dcp1a to promote its
376 degradation, but we speculate that post-translational modification of Dcp1a is involved. PB
377 proteins, including Dcp1a, EDC4/Hedls, Dcp2 and DDX6, are phosphorylated; however, the
378 functional consequences of these phosphorylation events for PB granule formation are not yet
379 fully appreciated (Bish *et al*, 2015; Gustafson & Wessel, 2010; Rahman *et al*, 2014; Yoon *et al*,
380 2010). Dcp1a is mono-phosphorylated at serine 315 which stabilizes its interaction with Dcp2;
381 however, hyperphosphorylation of Dcp1a coincided with PB loss, showing that Dcp1a
382 phosphorylation status regulates PB dynamics (Tenekeci *et al*, 2016; Aizer *et al*, 2013; Chiang *et*
383 *al*, 2013). PB proteins including Dcp1a, Dcp2 and EDC3 are also ubiquitinated, and

384 manipulation of total cellular K63-ubiquitination altered PB formation and function and changed
385 the mRNA half-life of selected cytokine transcripts in a gene-specific manner (Tenekeci *et al*,
386 2016). Our model is that KapB expression induces the post-translational modification of Dcp1a,
387 or a yet to be identified PB protein, to increase its recognition by NDP52, which then targets it to
388 nascent autophagosomes (model Fig 7). Future work will explore the interactome of NDP52
389 during KapB expression to determine Dcp1a post-translational modifications and whether other
390 PB proteins are modified or targeted for degradation.
391
392 In viral cancers like KS, autophagic flux promotes a pro-tumourigenic and pro-inflammatory
393 environment (Vescovo *et al*, 2020; Liu & Debnath, 2016; Pringle *et al*, 2019; Wu *et al*, 2012).
394 The data shown herein brings new understanding to this complex relationship during KSHV
395 infection. We show that KapB induces autophagic flux and NDP52 selective autophagy of PBs,
396 thereby supporting the pro-inflammatory environment associated with latent KSHV infection and
397 KS. The manipulation of NDP52 function and autophagic flux by KapB is yet another example
398 of the ingenuity with which viruses usurp cellular processes; revealing a regulatory network that
399 links NDP52 to inflammatory molecule production via PB catabolism.
400

401 **Materials and Methods**

402 **Cell culture**

403 All cells were grown at 37 °C with 5% CO_2 and 20% O_2. HEK293T cells (ATCC), HeLa Tet-Off
404 cells (Clontech), Atg5 +/+ and -/- MEFs (Kuma *et al*, 2004), HeLa Flp-In TREx GFP-Dcp1a
405 cells (a generous gift from Anne-Claude Gingras)(Youn *et al*, 2018), and iSLK.219 cells (a
406 generous gift from Don Ganem) (Myoung & Ganem, 2011) were cultured in DMEM (Thermo
407 Fisher) supplemented with 100 U/mL penicillin, 100 µg/mL streptomycin, 2 mM L-glutamine
408 (Thermo Fisher) and 10% FBS (Thermo Fisher). iSLK.219 cells were additionally cultured in the
409 presence of puromycin (10 µg/mL). HUVECs (Lonza) were cultured in endothelial cell growth
410 medium (EGM-2) (Lonza). HUVECs were seeded onto gelatin (1% w/v in PBS)-coated tissue
411 culture plates or glass coverslips. All drug treatments were performed for the times indicated in
412 each experiment at the concentrations listed in Table 1.

413 **Cloning**

414 All plasmids used in this study can be found in Table 2. All shRNAs were generated by cloning
415 shRNA hairpin sequences found in Table 3 into pLKO.1-TRC Puro (pLKO.1-TRC cloning
416 vector was a gift from David Root (Addgene plasmid # 10878; http://n2t.net/addgene:10878;
417 RRID:Addgene_10878) or pLKO.1-blast (pLKO.1-blast was a gift from Keith Mostov (Addgene
418 plasmid #26655; http://n2t.net/addgene:26655; RRID:Addgene_26655). pBMN mCherry-
419 NDP52(C443K) was a gift from Michael Lazarou (Addgene plasmid #119685;
420 http://n2t.net/addgene:119685; RRID:Addgene_119685) and pBMN mCherry-
421 NDP52(V136S/C443K) was a gift from Michael Lazarou (Addgene plasmid #119686;
422 http://n2t.net/addgene:119686; RRID:Addgene_119686). The overexpression plasmids, pLJM1

423 mCh-NDP52 C443K and pLJM1 mCh-NDP52 C443K V136S were made using the primers in
424 Table 4 to clone NDP52 into pLJM1 (Johnston *et al*, 2019).

425 **Lentivirus Production and Transduction**

426 All lentiviruses were generated using a second-generation system. Briefly, HEK293T cells were
427 transfected with pSPAX2, MD2G, and the plasmid containing a gene of interest or hairpin using
428 polyethylimine (PEI, Polysciences). psPAX2 was a gift from Didier Trono (Addgene plasmid
429 #12260; http://n2t.net/addgene:12260; RRID:Addgene_12260) and pMD2.G was a gift from
430 Didier Trono (Addgene plasmid #12259; http://n2t.net/addgene:12259; RRID:Addgene_12259).

431 Viral supernatants were harvested 48 h post-transfection, clarified using a 0.45 µm
432 polyethersulfone filter (VWR), and frozen at -80°C until use. For transduction, lentiviruses were
433 thawed at 37°C and added to target cells in complete media containing 5 µg/mL polybrene
434 (Sigma) for 24 h. The media was changed to selection media containing 1 µg/mL puromycin or 5
435 µg/mL blasticidin (Thermo) and cells were selected for 48 h before proceeding with
436 experiments.

437 **Viral conditioned media treatment**

438 iSLK.219 cells (latently infected with rKSHV.219 virus) (Vieira & O'Hearn, 2004) were sub-
439 cultured into a 10 mL cell culture dish and grown without puromycin for 72 h (Myoung &
440 Ganem, 2011). At 72 h, conditioned media was reserved and cleared of cellular debris by
441 centrifugation at 500 x g for 5 min. Supernatant was collected and filtered through a 0.22 µm
442 polyethersulfone (PES) membrane filter (VWR) and stored in aliquots at -80. Prior to the
443 experiment, conditioned media was thawed at 37°C and combined 1:1 with fresh HUVEC EGM-

444 2 media and used to treat vector or KapB-expressing HUVECs for 0 or 6 h prior to total RNA
445 harvest.

446 **Immunofluorescence**

447 Cells were seeded onto coverslips for immunofluorescence experiments and fixed for 10 mins at
448 37 °C in 4% (v/v) paraformaldehyde (Electron Microscopy Sciences). Samples were
449 permeabilized with 0.1% (v/v) Triton X-100 (Sigma-Aldrich) for 10 min at room temperature
450 and blocked in 1% human AB serum (Sigma-Aldrich) for 1 h at room temperature. For
451 autophagosome immunofluorescence cells were fixed for 10 min in ice cold methanol at -20 °C
452 and blocked in 1% human AB serum for 1 h at room temperature. Primary and secondary
453 antibodies were diluted in 1% human AB serum and used at the concentrations in Table 5.
454 Samples were mounted with Prolong Gold AntiFade mounting media (Thermo). For CellProfiler
455 quantification of puncta, samples were incubated with WGA AlexaFluor-647 at a 1:400 dilution
456 for 10 min prior to permeabilization. Image analysis was performed using CellProfiler
457 (cellprofiler.org), an open source platform for image analysis (Carpenter *et al*, 2006);
458 quantification of puncta was performed as previously described, with the exception that cells
459 were defined by propagating out a set number of pixels from each nucleus (Castle *et al*, 2021).

460 **Immunoblotting**

461 Cells were lysed in 2x Laemmli buffer and stored at -20°C until use. The DC Protein Assay
462 (Bio-Rad) was used to quantify protein concentration as per the manufacturer's instructions. 10-
463 15 µg of protein lysate was resolved by SDS-PAGE on TGX Stain-Free acrylamide gels
464 (BioRad). Total protein images were acquired from the PVDF membranes after transfer on the
465 ChemiDoc Touch Imaging system (BioRad). Membranes were blocked in 5% bovine serum

466 albumin (BSA) or skim milk in Tris-buffered saline-Tween20 (TBS-T). Primary and secondary
467 antibodies were diluted in 2.5% BSA or skim milk; antibody dilutions can be found in Table 5.
468 Membranes were visualized using Clarity Western ECL substrate and the ChemiDoc Touch
469 Imaging system (BioRad).

470 **Luciferase Assays**

471 Luciferase assays were performed as previously described (Corcoran *et al*, 2011). HeLa Tet-Off
472 cells were transduced with recombinant lentivirus expressing different shRNAs and selected.
473 Cells were transfected according to Corcoran *et al.* (2011) with pTRE2 Firefly Luciferase ARE,
474 pTRE2 Renilla Luciferase, and the expression plasmid of interest using Fugene HD (Promega).
475 Luciferase and renilla activity were quantified using the Dual Luciferase Assay Kit (Promega)
476 and read on a GloMax multi-detection system (Promega).

477 **Quantitative PCR**

478 RNA was collected using a RNeasy Plus Mini Kit (Qiagen) according to the manufacturer's
479 instructions and stored at -80°C until further use. RNA concentration was determined and was
480 reverse transcribed using Maxima H Minus First Strand cDNA Synthesis Kit (Thermo Fisher)
481 using a combination of random and oligo (dT) primers according to the manufacturer's
482 instructions. cDNA was diluted 1:5 for all qPCR experiments and GoTaq qPCR Master Mix
483 (Promega) was used to amplify cDNA. The ΔΔ-Quantitation cycle (Cq) method was used to
484 determine the fold change in expression of target transcripts. qPCR primer sequences can be
485 found in Table 6.

486 **Statistics**

487 Data shown are the mean ± standard error of the mean (SEM). Statistical significance was
488 determined using a one-way ANOVA, a 2-way ANOVA or Student's t-test when appropriate
489 with the applicable post-test (indicated in the corresponding figure legends). For ANOVAs,
490 matched data from each replicate was paired for analysis. All statistics were performed using
491 GraphPad Prism v.9.0.

492

493

494 **Acknowledgements**

495 The authors would like to dedicate this manuscript to Dr. Beth Levine, who was a leader in the
496 field of autophagy and viruses and who inspired this work. We sincerely thank the members of
497 the Corcoran lab for helpful discussions about this work. We would like to thank Dr. Craig
498 McCormick (Dalhousie University), Dr. Eric Pringle (Dalhousie University), and Dr. Andrew
499 Leidal (UCSF) for valuable feedback on this manuscript and the McCormick lab for plasmids,
500 expertise and advice. We would like to thank Mr. Stephen Whitefield and Ms. Mary Ann Trevors
501 in the Dalhousie *CORES* (Cellular and Molecular Digital Imaging and Electron Microscopy core
502 facilities) and Dr. Anne Vaahtokari of the Charbonneau Microscopy Facility, UCalgary for
503 microscopy support. We would like to thank Dr. Andreas Till (University of Bonn), Dr. Anne-
504 Claude Gingras (Lunenfeld-Tanenbaum Research Institute) and Dr. Don Ganem (Novartis) for
505 sharing valuable reagents. Model figure created with BioRender. GKS was supported by a CIHR
506 CGS-M scholarship and Scotia Scholars NSHRF graduate training award. ELC was supported by
507 a Killam predoctoral scholarship, an NSERC CGS-M scholarship, and a Nova Scotia Graduate
508 scholarship. Operating funds to support this work derive from a CIHR Project Grant PJT-153210
509 to JAC.

510

511 **Author Contributions**

512 Carolyn-Ann Robinson: Conceptualization, Experimentation, Analysis, Paper Writing

513 Gillian K. Singh: Conceptualization, Experimentation, Analysis, Paper Writing

514 Elizabeth L. Castle: Analysis

Bre Q. Boudreau: Experimentation

Jennifer A. Corcoran: Conceptualization, Experimentation, Supervision, Funding Acquisition, Project Administration, Paper Writing

Conflict of Interest

The authors have no competing interests to declare.

523 **References**
524

525 Ahmad L, Mostowy S & Sancho-Shimizu V (2018) Autophagy-virus interplay: From cell
526 biology to human disease. *Front Cell Dev Biol* 6 doi:10.3389/fcell.2018.00155
527 [PREPRINT]

528 Aizer A, Kafri P, Kalo A & Shav-Tal Y (2013) The P Body Protein Dcp1a Is Hyper-
529 phosphorylated during Mitosis. *PLoS One* 8: e49783

530 Ayache J, Bénard M, Ernoult-Lange M, Minshall N, Standart N, Kress M & Weil D (2015) P-
531 body assembly requires DDX6 repression complexes rather than decay or Ataxin2/2L
532 complexes. *Mol Biol Cell* 26: 2579–2595

533 Bakheet T, Hitti E & Khabar KSA (2018) ARED-Plus: An updated and expanded database of
534 AU-rich element-containing mRNAs and pre-mRNAs. *Nucleic Acids Res* 46: D218–D220

535 Balgi AD, Fonseca BD, Donohue E, Tsang TCF, Lajoie P, Proud CG, Nabi IR & Roberge M
536 (2009) Screen for chemical modulators of autophagy reveals novel therapeutic inhibitors of
537 mTORC1 signaling. *PLoS One* 4

538 Barreau C, Paillard L & Osborne HB (2005) AU-rich elements and associated factors: Are there
539 unifying principles? *Nucleic Acids Res* 33: 7138–7150 doi:10.1093/nar/gki1012
540 [PREPRINT]

541 Birgisdottir ÅB, Lamark T & Johansen T (2013) The LIR motif - crucial for selective autophagy.
542 *J Cell Sci* 126: 3237–47

543 Bish R, Cuevas-Polo N, Cheng Z, Hambardzumyan D, Munschauer M, Landthaler M & Vogel C
544 (2015) Comprehensive Protein Interactome Analysis of a Key RNA Helicase: Detection of
545 Novel Stress Granule Proteins. *Biomolecules* 5: 1441–66

546 Blanco FF, Sanduja S, Deane NG, Blackshear PJ & Dixon D a (2014) Transforming growth
547 factor β regulates P-body formation through induction of the mRNA decay factor
548 tristetraprolin. *Mol Cell Biol* 34: 180–95

549 Broussard G & Damania B (2020) Regulation of KSHV Latency and Lytic Reactivation. *Viruses*
550 12 doi:10.3390/v12091034 [PREPRINT]

551 Buchan JR, Kolaitis R, Taylor JP & Parker R (2013) Eukaryotic Stress Granules Are Cleared by
552 Autophagy and Cdc48 / VCP Function. *Cell* 153: 1461–1474

553 Carpenter AE, Jones TR, Lamprecht MR, Clarke C, Kang I, Friman O, Guertin DA, Chang J,
554 Lindquist RA, Moffat J, *et al* (2006) CellProfiler: image analysis software for identifying
555 and quantifying cell phenotypes. *Genome Biol* 7: R100

556 Castle EL, Robinson C-A, Douglas P, Rinker KD & Corcoran JA (2021) Viral manipulation of a
557 mechanoresponsive signaling axis disassembles processing bodies. *bioRxiv*:
558 2020.05.15.091876

559 Cemma M, Kim PK & Brumell JH (2011) The ubiquitin-binding adaptor proteins p62/SQSTM1
560 and NDP52 are recruited independently to bacteria-associated microdomains to target

561 Salmonella to the autophagy pathway. *Autophagy* 7: 341–5

562 Cesarman E, Chang Y, Moore PS, Said JW & Knowles DM (1995) Kaposi's sarcoma-associated
563 herpesvirus-like DNA sequences in AIDS-related body-cavity-based lymphomas. *N Engl J*
564 *Med* 332: 1186–1191

565 Chang Y, Cesarman E, Pessin MS, Lee F, Culpepper J, Knowles DM & Moore PS (1994)
566 Identification of herpesvirus-like DNA sequences in AIDS-associated Kaposi's sarcoma.
567 *Science* 266: 1865–9

568 Chen M, Meng Q, Qin Y, Liang P, Tan P, He L, Zhou Y, Chen Y, Huang J, Wang RF, *et al*
569 (2016) TRIM14 Inhibits cGAS Degradation Mediated by Selective Autophagy Receptor
570 p62 to Promote Innate Immune Responses. *Mol Cell* 64: 105–119

571 Chiang PY, Shen YF, Su YL, Kao CH, Lin NY, Hsu PH, Tsai MD, Wang SC, Chang GD, Lee
572 SC, *et al* (2013) Phosphorylation of mRNA Decapping Protein Dcp1a by the ERK
573 Signaling Pathway during Early Differentiation of 3T3-L1 Preadipocytes. *PLoS One* 8

574 Corbet GA & Parker R (2019) RNP granule formation: Lessons from P-bodies and stress
575 granules. *Cold Spring Harb Symp Quant Biol* 84: 203–215

576 Corcoran JA, Johnston BP & McCormick C (2015) Viral activation of MK2-hsp27-
577 p115RhoGEF-RhoA signaling axis causes cytoskeletal rearrangements, p-body disruption
578 and ARE-mRNA stabilization. *PLoS Pathog* 11: e1004597

579 Corcoran JA, Khaperskyy DA, Johnston BP, King CA, Cyr DP, Olsthoorn A V. & McCormick
580 C (2012) Kaposi's Sarcoma-Associated Herpesvirus G-Protein-Coupled Receptor Prevents
581 AU-Rich-Element-Mediated mRNA Decay. *J Virol* 86: 8859–8871

582 Corcoran JA, Khaperskyy DA & McCormick C (2011) Assays for monitoring viral manipulation
583 of host ARE-mRNA turnover. *Methods* 55: 172–181

584 Corcoran JA & McCormick C (2015) Viral activation of stress-regulated Rho-GTPase signaling
585 pathway disrupts sites of mRNA degradation to influence cellular gene expression. *Small*
586 *GTPases* 6: 178–185 doi:10.1080/21541248.2015.1093068 [PREPRINT]

587 Cougot N, Cavalier A, Thomas D & Gillet R (2012) The Dual Organization of P-bodies
588 Revealed by Immunoelectron Microscopy and Electron Tomography. *J Mol Biol* 420: 17–
589 28

590 Decker LL, Shankar P, Khan G, Freeman RB, Dezube BJ, Lieberman J & Thorley-Lawson DA
591 (1996) The Kaposi sarcoma-associated herpesvirus (KSHV) is present as an intact latent
592 genome in KS tissue but replicates in the peripheral blood mononuclear cells of KS patients.
593 *J Exp Med* 184: 283–8

594 Docena G, Rovedatti L, Kruidenier L, Fanning Á, Leakey NAB, Knowles CH, Lee K, Shanahan
595 F, Nally K, McLean PG, *et al* (2010) Down-regulation of p38 mitogen-activated protein
596 kinase activation and proinflammatory cytokine production by mitogen-activated protein
597 kinase inhibitors in inflammatory bowel disease. *Clin Exp Immunol* 162: 108–115

598 Dougherty JD, White JP & Lloyd RE (2011) Poliovirus-mediated disruption of cytoplasmic
599 processing bodies. *J Virol* 85: 64–75

600 Du Y, Duan T, Feng Y, Liu Q, Lin M, Cui J & Wang R (2018) LRRC25 inhibits type I IFN
601 signaling by targeting ISG15-associated RIG-I for autophagic degradation. *EMBO J* 37:
602 351–366

603 Dunn WA, Cregg JM, Kiel JAKW, van der Klei IJ, Oku M, Sakai Y, Sibirny AA, Stasyk O V. &
604 Veenhuis M (2005) Pexophagy: the selective autophagy of peroxisomes. *Autophagy* 1: 75–
605 83 doi:10.4161/auto.1.2.1737 [PREPRINT]

606 Ellinghaus D, Zhang H, Zeissig S, Lipinski S, Till A, Jiang T, Stade B, Bromberg Y, Ellinghaus
607 E, Keller A, *et al* (2013) Association between variants of PRDM1 and NDP52 and Crohn's
608 disease, based on exome sequencing and functional studies. *Gastroenterology* 145: 339–47

609 Ensoli B, Nakamura S, Salahuddin SZ, Biberfeld P, Larsson L, Beaver B, Wong-staal F & Gallo
610 RC (2010) AIDS-Kaposi's Sarcoma-Derived Cells Express Cytokines with Autocrine and
611 Paracrine Growth Effects. *Science (80-)* 243: 223–226

612 Ensoli B & Stürzl M (1998) Kaposi's sarcoma: a result of the interplay among inflammatory
613 cytokines, angiogenic factors and viral agents. *Cytokine Growth Factor Rev* 9: 63–83

614 Franks TM & Lykke-Andersen J (2007) TTP and BRF proteins nucleate processing body
615 formation to silence mRNAs with AU-rich elements. *Genes Dev* 21: 719–735

616 Franks TM & Lykke-Andersen J (2008) The control of mRNA decapping and P-body formation.
617 *Mol Cell* 32: 605–15

618 Fu T, Liu J, Wang Y, Xie X, Hu S & Pan L (2018) Mechanistic insights into the interactions of
619 NAP1 with the SKICH domains of NDP52 and TAX1BP1. *Proc Natl Acad Sci U S A* 115:
620 E11651–E11660

621 García-Mauriño SM, Rivero-Rodríguez F, Velázquez-Cruz A, Hernández-Vellisca M, Díaz-
622 Quintana A, De la Rosa MA & Díaz-Moreno I (2017) RNA binding protein regulation and
623 cross-talk in the control of AU-rich mRNA Fate. *Front Mol Biosci* 4: 71
624 doi:10.3389/fmolb.2017.00071 [PREPRINT]

625 Green DR, Galluzzi L & Kroemer G (2011) Mitochondria and the autophagy-inflammation-cell
626 death axis in organismal aging. *Science (80-)* 333: 1109–1112
627 doi:10.1126/science.1201940 [PREPRINT]

628 Guo H, Chitiprolu M, Gagnon D, Meng L, Perez-Iratxeta C, Lagace D & Gibbings D (2014)
629 Autophagy supports genomic stability by degrading retrotransposon RNA. *Nat Commun* 5:
630 5276

631 Guo L, Louis IV-S & Bohjanen PR (2018) Post-transcriptional regulation of cytokine expression
632 and signaling. *Curr Trends Immunol* 19: 33–40

633 Gurkar AU, Chu K, Raj L, Bouley R, Lee S-H, Kim Y-B, Dunn SE, Mandinova A & Lee SW
634 (2013) Identification of ROCK1 kinase as a critical regulator of Beclin1-mediated
635 autophagy during metabolic stress. *Nat Commun* 4: 2189

636 Gustafson EA & Wessel GM (2010) DEAD-box helicases: posttranslational regulation and
637 function. *Biochem Biophys Res Commun* 395: 1–6

638 Hardy SD, Shinde A, Wang W-H, Wendt MK & Geahlen RL (2017) Regulation of epithelial-
639 mesenchymal transition and metastasis by TGF-β, P-bodies, and autophagy. *Oncotarget* 8:
640 103302–103314

641 He X, Zhu Y, Zhang Y, Geng Y, Gong J, Geng J, Zhang P, Zhang X, Liu N, Peng Y, *et al* (2019)
642 RNF 34 functions in immunity and selective mitophagy by targeting MAVS for autophagic
643 degradation . *EMBO J* 38

644 Hubstenberger A, Courel M, Bénard M, Souquere S, Ernoult-Lange M, Chouaib R, Yi Z, Morlot
645 J-B, Munier A, Fradet M, *et al* (2017) P-Body Purification Reveals the Condensation of
646 Repressed mRNA Regulons. *Mol Cell* 68: 144-157.e5

647 Ichimura Y, Kumanomidou T, Sou Y, Mizushima T, Ezaki J, Ueno T, Kominami E, Yamane T,
648 Tanaka K & Komatsu M (2008) Structural basis for sorting mechanism of p62 in selective
649 autophagy. *J Biol Chem* 283: 22847–57

650 Jin S, Tian S, Luo M, Xie W, Liu T, Duan T, Wu Y & Cui J (2017) Tetherin Suppresses Type I
651 Interferon Signaling by Targeting MAVS for NDP52-Mediated Selective Autophagic
652 Degradation in Human Cells. *Mol Cell* 68: 308-322.e4

653 Johnston BP, Pringle ES & McCormick C (2019) KSHV activates unfolded protein response
654 sensors but suppresses downstream transcriptional responses to support lytic replication.
655 *PLoS Pathog* 15

656 Kabeya Y (2000) LC3, a mammalian homologue of yeast Apg8p, is localized in autophagosome
657 membranes after processing. *EMBO J* 19: 5720–5728

658 Katayama H, Yamamoto A, Mizushima N, Yoshimori T & Miyawaki A (2008) GFP-like
659 proteins stably accumulate in lysosomes. *Cell Struct Funct* 33: 1–12

660 Kayyali US, Pennella CM, Trujillo C, Villa O, Gaestel M & Hassoun PM (2002) Cytoskeletal
661 changes in hypoxic pulmonary endothelial cells are dependent on MAPK-activated protein
662 kinase MK2. *J Biol Chem* 277: 42596–42602

663 Kenific CM, Stehbens SJ, Goldsmith J, Leidal AM, Faure N, Ye J, Wittmann T & Debnath J
664 (2016) NBR 1 enables autophagy-dependent focal adhesion turnover. *J Cell Biol* 212: 577–
665 590

666 Klionsky DJ, Abdalla FC, Abeliovich H, Abraham RT, Acevedo-Arozena A, Adeli K, Agholme
667 L, Agnello M, Agostinis P, Aguirre-Ghiso JA, *et al* (2012) Guidelines for the use and
668 interpretation of assays for monitoring autophagy. *Autophagy* 8: 445–544

669 Kuma A, Hatano M, Matsui M, Yamamoto A, Nakaya H, Yoshimori T, Ohsumi Y, Tokuhisa T
670 & Mizushima N (2004) The role of autophagy during the early neonatal starvation period.
671 *Nature* 432: 1032–1036

672 Lai WS & Blackshear PJ (2001) Interactions of CCCH zinc finger proteins with mRNA.
673 Tristetraprolin-mediated AU-rich element-dependent mRNA degradation can occur in the
674 absence of a poly(A) tail. *J Biol Chem* 276: 23144–23154

675 Lai WS, Carballo E, Strum JR, Kennington EA, Phillips RS & Blackshear PJ (1999) Evidence
676 that Tristetraprolin Binds to AU-Rich Elements and Promotes the Deadenylation and

677 Destabilization of Tumor Necrosis Factor Alpha mRNA. *Mol Cell Biol* 19: 4311–4323

678 Lane BR, Liu J, Bock PJ, Schols D, Coffey MJ, Strieter RM, Polverini PJ & Markovitz DM
679 (2002) Interleukin-8 and growth-regulated oncogene alpha mediate angiogenesis in
680 Kaposi's sarcoma. *J Virol* 76: 11570–83

681 Lazarou M, Sliter DA, Kane LA, Sarraf SA, Wang C, Burman JL, Sideris DP, Fogel AI & Youle
682 RJ (2015) The ubiquitin kinase PINK1 recruits autophagy receptors to induce mitophagy.
683 *Nature* 524: 309–314

684 Lee J-S, Li Q, Lee J-Y, Lee S-H, Jeong JH, Lee H-R, Chang H, Zhou F-C, Gao S-J, Liang C, *et*
685 *al* (2009) FLIP-mediated autophagy regulation in cell death control. *Nat Cell Biol* 11: 1355–
686 1362

687 Leidal AM, Cyr DP, Hill RJ, Lee PWK & McCormick C (2012) Subversion of autophagy by
688 Kaposi's sarcoma-associated herpesvirus impairs oncogene-induced senescence. *Cell Host*
689 *Microbe* 11: 167–180

690 Levine B, Sinha S & Kroemer G (2008) Bcl-2 family members: Dual regulators of apoptosis and
691 autophagy. *Autophagy* 4: 600–606 doi:10.4161/auto.6260 [PREPRINT]

692 Liu J & Debnath J (2016) The Evolving, Multifaceted Roles of Autophagy in Cancer. In
693 *Advances in Cancer Research* pp 1–53. Academic Press Inc.

694 Liu Q, Xu C, Kirubakaran S, Zhang X, Hur W, Liu Y, Kwiatkowski NP, Wang J, Westover KD,
695 Gao P, *et al* (2013) Characterization of Torin2, an ATP-competitive inhibitor of mTOR,
696 ATM, and ATR. *Cancer Res* 73: 2574–2586

697 Luo Y, Na Z & Slavoff SA (2018) P-Bodies: Composition, Properties, and Functions.
698 *Biochemistry* 57: 2424

699 Maitra S, Chou CF, Luber CA, Lee KY, Mann M & Chen CY (2008) The AU-rich element
700 mRNA decay-promoting activity of BRF1 is regulated by mitogen-activated protein kinase-
701 activated protein kinase 2. *RNA* 14: 950–959

702 Maiuri MC & Kroemer G (2015) Autophagy in stress and disease. *Cell Death Differ* 22: 365–
703 366 doi:10.1038/cdd.2014.236 [PREPRINT]

704 Mauvezin C & Neufeld TP (2015) Bafilomycin A1 disrupts autophagic flux by inhibiting both
705 V-ATPase-dependent acidification and Ca-P60A/SERCA-dependent autophagosome-
706 lysosome fusion. *Autophagy* 11: 1437–1438

707 McCormick C & Ganem D (2005) The Kaposin B Protein of KSHV Activates the p38/MK2
708 Pathway and Stabilizes Cytokine mRNAs. *Science (80-)* 307: 739–741

709 Miles SA, Rezai AR, Salazar-González JF, Vander Meyden M, Stevens RH, Logan DM,
710 Mitsuyasu RT, Taga T, Hirano T & Kishimoto T (1990) AIDS Kaposi sarcoma-derived
711 cells produce and respond to interleukin 6. *Proc Natl Acad Sci U S A* 87: 4068–72

712 Mizushima N, Yoshimori T & Levine B (2010) Methods in Mammalian Autophagy Research.
713 *Cell* 140: 313–326 doi:10.1016/j.cell.2010.01.028 [PREPRINT]

714 Mohamud Y, Qu J, Xue YC, Liu H, Deng H & Luo H (2019) CALCOCO2/NDP52 and

715 SQSTM1/p62 differentially regulate coxsackievirus B3 propagation. *Cell Death Differ* 26:
716 1062–1076

717 Morishita H & Mizushima N (2019) Diverse cellular roles of autophagy. *Annu Rev Cell Dev Biol*
718 35: 453–475 doi:10.1146/annurev-cellbio-100818-125300 [PREPRINT]

719 Morriswood B, Ryzhakov G, Puri C, Arden SD, Roberts R, Dendrou C, Kendrick-Jones J &
720 Buss F (2007) T6BP and NDP52 are myosin VI binding partners with potential roles in
721 cytokine signalling and cell adhesion. *J Cell Sci* 120: 2574–85

722 Myoung J & Ganem D (2011) iSLK cell. *J Virol Methods* 174: 12–21

723 Noda NN, Kumeta H, Nakatogawa H, Satoo K, Adachi W, Ishii J, Fujioka Y, Ohsumi Y &
724 Inagaki F (2008) Structural basis of target recognition by Atg8/LC3 during selective
725 autophagy. *Genes to Cells* 13: 1211–1218

726 Noda NN, Ohsumi Y & Inagaki F (2010) Atg8-family interacting motif crucial for selective
727 autophagy. *FEBS Lett* 584: 1379–1385

728 Padman BS, Nguyen TN, Uoselis L, Skulsuppaisarn M, Nguyen LK & Lazarou M (2019)
729 LC3/GABARAPs drive ubiquitin-independent recruitment of Optineurin and NDP52 to
730 amplify mitophagy. *Nat Commun* 10: 1–13

731 Prabakaran T, Bodda C, Krapp C, Zhang B, Christensen MH, Sun C, Reinert L, Cai Y, Jensen
732 SB, Skouboe MK, *et al* (2018) Attenuation of c GAS - STING signaling is mediated by a
733 p62/ SQSTM 1-dependent autophagy pathway activated by TBK1 . *EMBO J* 37

734 Pringle ES, Robinson C-A & McCormick C (2019) Kaposi's Sarcoma-Associated Herpesvirus
735 Lytic Replication Interferes with mTORC1 Regulation of Autophagy and Viral Protein
736 Synthesis. *J Virol* 93

737 Rahman H, Qasim M, Oellerich M & Asif AR (2014) Crosstalk between Edc4 and mammalian
738 target of rapamycin complex 1 (mTORC1) signaling in mRNA decapping. *Int J Mol Sci* 15:
739 23179–95

740 Riggs CL, Kedersha N, Ivanov P & Anderson P (2020) Mammalian stress granules and P bodies
741 at a glance. *J Cell Sci* 133 doi:10.1242/jcs.242487 [PREPRINT]

742 Riva G, Barozzi P, Torelli G & Luppi M (2010) Immunological and Inflammatory Features of
743 Kaposi's Sarcom and Other Kaposi's Sarcoma-Associated Herpesvirus/Human Herpesvirus
744 8-Associated Neoplasias. *AIDS Rev* 9: 25–39

745 Rogov V, Dötsch V, Johansen T & Kirkin V (2014) Interactions between Autophagy Receptors
746 and Ubiquitin-like Proteins Form the Molecular Basis for Selective Autophagy. *Mol Cell*
747 53: 167–178

748 Rousseau S, Houle F, Landry J & Huot J (1997) P38 MAP kinase activation by vascular
749 endothelial growth factor mediates actin reorganization and cell migration in human
750 endothelial cells. *Oncogene* 15: 2169–2177

751 Sadagopan S, Sharma-Walia N, Veettil MV, Raghu H, Sivakumar R, Bottero V & Chandran B
752 (2007) Kaposi's Sarcoma-Associated Herpesvirus Induces Sustained NF-κB Activation

753 during De Novo Infection of Primary Human Dermal Microvascular Endothelial Cells That
754 Is Essential for Viral Gene Expression. *J Virol* 81: 3949–3968

755 Salahuddin S, Nakamura S, Biberfeld P, Kaplan M, Markham P, Larsson L & Gallo R (1988)
756 Angiogenic properties of Kaposi's sarcoma-derived cells after long-term culture in vitro.
757 *Science (80-)* 242: 430–433

758 Sargsyan A, Cai J, Fandino LB, Labasky ME, Forostyan T, Colosimo LK, Thompson SJ &
759 Graham TE (2015) Rapid parallel measurements of macroautophagy and mitophagy in
760 mammalian cells using a single fluorescent biosensor. *Sci Rep* 5

761 Seth RB, Sun L, Ea CK & Chen ZJ (2005) Identification and characterization of MAVS, a
762 mitochondrial antiviral signaling protein that activates NF-κB and IRF3. *Cell* 122: 669–682

763 Shen L, Qi Z, Zhu Y, Song X, Xuan C, Ben P, Lan L, Luo L & Yin Z (2016) Phosphorylated
764 heat shock protein 27 promotes lipid clearance in hepatic cells through interacting with
765 STAT3 and activating autophagy. *Cell Signal* 28: 1086–1098

766 Soulier J, Grollet L, Oksenhendler E, Cacoub P, Cazals-Hatem D, Babinet P, d'Agay MF,
767 Clauvel JP, Raphael M & Degos L (1995) Kaposi's sarcoma-associated herpesvirus-like
768 DNA sequences in multicentric Castleman's disease. *Blood* 86: 1276–80

769 Standart N & Weil D (2018) P-Bodies: Cytosolic Droplets for Coordinated mRNA Storage.
770 *Trends Genet* 34: 612–626 doi:10.1016/j.tig.2018.05.005 [PREPRINT]

771 Staskus KA, Zhong W, Gebhard K, Herndier B, Wang H, Renne R, Beneke J, Pudney J,
772 Anderson DJ, Ganem D, *et al* (1997) Kaposi's sarcoma-associated herpesvirus gene
773 expression in endothelial (spindle) tumor cells. *J Virol* 71: 715–9

774 Sumpter R & Levine B (2011) Selective autophagy and viruses. *Autophagy* 7: 260–265
775 doi:10.4161/auto.7.3.14281 [PREPRINT]

776 Tenekeci U, Poppe M, Beuerlein K, Busch J, Schmitz ML & Kracht Correspondence M (2016)
777 K63-Ubiquitylation and TRAF6 Pathways Regulate Mammalian P-Body Formation and
778 mRNA Decapping. *Mol Cell* 62: 943–957

779 Thoreen CC, Kang SA, Won Chang J, Liu Q, Zhang J, Gao Y, Reichling LJ, Sim T, Sabatini DM
780 & Gray NS (2009) An ATP-competitive Mammalian Target of Rapamycin Inhibitor
781 Reveals Rapamycin-resistant Functions of mTORC1 * □ S. *J Biol Chem* 284: 8023–32

782 Till A, Lipinski S, Ellinghaus D, Mayr G, Subramani S, Rosenstiel P & Franke A (2013)
783 Autophagy receptor CALCOCO2/NDP52 takes center stage in Crohn disease. *Autophagy* 9:
784 1256–7

785 Tripathi DN, Zhang J, Jing J, Dere R & Walker CL (2016) A new role for ATM in selective
786 autophagy of peroxisomes (pexophagy). *Autophagy* 12: 711–712
787 doi:10.1080/15548627.2015.1123375 [PREPRINT]

788 Turakhiya A, Meyer SR, Marincola G, Böhm S, Vanselow JT, Schlosser A, Hofmann K &
789 Buchberger A (2018) ZFAND1 Recruits p97 and the 26S Proteasome to Promote the
790 Clearance of Arsenite-Induced Stress Granules. *Mol Cell* 70: 906-919.e7

791 Verlhac P, Gré IP, Viret C & Faure M (2015) Autophagy Receptor NDP52 Regulates Pathogen-
792 Containing Autophagosome Maturation. *Cell Host Microbe* 17: 515–525

793 Vescovo T, Pagni B, Piacentini M, Fimia GM & Antonioli M (2020) Regulation of Autophagy in
794 Cells Infected With Oncogenic Human Viruses and Its Impact on Cancer Development.
795 *Front Cell Dev Biol* 8 doi:10.3389/fcell.2020.00047 [PREPRINT]

796 Vieira J & O'Hearn PM (2004) Use of the red fluorescent protein as a marker of Kaposi's
797 sarcoma-associated herpesvirus lytic gene expression. *Virology* 325: 225–240

798 Vindry C, Marnef A, Broomhead H, Twyffels L, Ozgur S, Stoecklin G, Llorian M, Smith CW,
799 Mata J, Weil D, *et al* (2017) Dual RNA Processing Roles of Pat1b via Cytoplasmic Lsm1-7
800 and Nuclear Lsm2-8 Complexes. *Cell Rep* 20: 1187–1200

801 Wei Y, An Z, Zou Z, Sumpter R, Su M, Zang X, Sinha S, Gaestel M & Levine B (2015) The
802 stress-responsive kinases MAPKAPK2/MAPKAPK3 activate starvation-induced autophagy
803 through Beclin 1 phosphorylation. *Elife* 4

804 Wen KW & Damania B (2010) Kaposi sarcoma-associated herpesvirus (KSHV): molecular
805 biology and oncogenesis. *Cancer Lett* 289: 140–50

806 Wu WKK, Coffelt SB, Cho CH, Wang XJ, Lee CW, Chan FKL, Yu J & Sung JJY (2012) The
807 autophagic paradox in cancer therapy. *Oncogene* 31: 939–953 doi:10.1038/onc.2011.295
808 [PREPRINT]

809 Wu Y, Jin S, Liu Q, Zhang Y, Ma L, Zhao Z, Yang S, Li YP & Cui J (2020) Selective autophagy
810 controls the stability of transcription factor IRF3 to balance type I interferon production and
811 immune suppression. *Autophagy*

812 Xie X, Li F, Wang Y, Wang Y, Lin Z, Cheng X, Liu J, Chen C & Pan L (2015) Molecular basis
813 of ubiquitin recognition by the autophagy receptor CALCOCO2. *Autophagy* 11: 1775–89

814 Yang Q, Liu TT, Lin H, Zhang M, Wei J, Luo WW, Hu YH, Zhong B, Hu MM & Shu HB
815 (2017) TRIM32-TAX1BP1-dependent selective autophagic degradation of TRIF negatively
816 regulates TLR3/4-mediated innate immune responses. *PLoS Pathog* 13

817 Yao Z & Klionsky DJ (2016) An unconventional pathway for mitochondrial protein degradation.
818 *Autophagy* 12: 1971–1972 doi:10.1080/15548627.2016.1235127 [PREPRINT]

819 Yoon J-H, Choi E-J & Parker R (2010) Dcp2 phosphorylation by Ste20 modulates stress granule
820 assembly and mRNA decay in Saccharomyces cerevisiae. *J Cell Biol* 189: 813–27

821 Youn JY, Dunham WH, Hong SJ, Knight JDR, Bashkurov M, Chen GI, Bagci H, Rathod B,
822 MacLeod G, Eng SWM, *et al* (2018) High-Density Proximity Mapping Reveals the
823 Subcellular Organization of mRNA-Associated Granules and Bodies. *Mol Cell* 69: 517-
824 532.e11

825 Young ARJ, Narita M, Ferreira M, Kirschner K, Sadaie M, Darot JFJ, Tavaré S, Arakawa S,
826 Shimizu S, Watt FM, *et al* (2009) Autophagy mediates the mitotic senescence transition.
827 *Genes Dev* 23: 798–803

828 Zaffagnini G & Martens S (2016) Mechanisms of Selective Autophagy. *J Mol Biol* 428: 1714–

1724

832 **Figure Legends**

833 **Figure 1: Kaposin B requires canonical autophagy to disassemble PBs.** Primary human
834 umbilical vein endothelial cells (HUVECs) were transduced with recombinant lentiviruses
835 expressing either Kaposin B (KapB) or an empty vector control and selected with blasticidin (5
836 µg/mL). A: Cells were treated with bafilomycin A1 (10 nM) or a vehicle control (DMSO) for
837 the indicated times prior to harvest in 2x Laemmli buffer. Protein lysates were resolved by SDS-
838 PAGE and immunoblot was performed for p62 and LC3. Samples were quantified using Image
839 Lab (Biorad) software and then normalized, first to total protein and then to their respective
840 starting time points (0 h). Results were plotted in GraphPad and a linear regression statistical
841 test was performed, ±SEM; n=3, *=P<0.05, ***=P<0.001. B: Cells were treated with BafA1 for
842 30 min prior to fixation in methanol. Immunofluorescence was performed for LC3 (white) and
843 DAPI (nuclei, blue). Scale bar=20 µm. Total LC3 area per field was quantified by identifying
844 LC3-positive puncta using CellProfiler and normalizing to the number of nuclei and the vector
845 DMSO control. Results were plotted in GraphPad, a 2-way ANOVA was performed with a
846 Šidák's multiple comparison test, ±SEM; n=3, *=P<0.05. C: HUVECs were sequentially
847 transduced: first with recombinant lentiviruses expressing either shRNAs targeting Atg5 or
848 Atg14 (shAtg5, shAtg14) or a non-targeting control (NS) and selected with puromycin (1
849 µg/mL), and second with either KapB or an empty vector control and selected with blasticidin (5
850 µg/mL). Coverslips were fixed in 4% paraformaldehyde, permeabilized in 0.1% Triton X-100,
851 and immunostained for the PB-resident protein Hedls (white) and nuclei (DAPI). Scale bar=20
852 µm. Hedls puncta were quantified using CellProfiler and normalized to the number of nuclei,
853 results were plotted in GraphPad and a 2-way ANOVA was performed with a Šidák's multiple
854 comparison test, ±SEM; n=3, *=P<0.05. D: HUVECs were transduced as in A and treated with

855 DMSO or bafilomycin A1 (10 nM) for 30 min before being fixed in 4% paraformaldehyde and
856 permeabilized in 0.1% Triton X-100. Immunofluorescence was performed for Hedls (PBs,
857 white) and DAPI (nuclei, blue). Scale bar=20 µm. Hedls puncta were counted using CellProfiler
858 and normalized to the number of nuclei, results were plotted in GraphPad and a 2-way ANOVA
859 was performed with a Šidák's multiple comparison test, ±SEM; n=3, *=P<0.05.

860 **Figure 2: Torin treatment disassembles PBs.** A: HUVECs were treated with either Torin (250
861 nM) or a DMSO control for 2 h prior to fixation in 4% paraformaldehyde. Samples were
862 permeabilized in 0.1% Triton X-100. Immunofluorescence was performed for Hedls (PBs,
863 white) and DAPI (nuclei, blue). Scale bar=20 µm. Hedls puncta were counted using CellProfiler
864 and normalized to the number of nuclei, results were plotted in GraphPad and a 2-way ANOVA
865 was performed with a Šidák's multiple comparison test, ±SEM; n=3, *=P<0.05. B: HUVECs
866 were treated with either Torin (250 nM) or a DMSO control for 90 min prior to the addition of
867 sodium arsenite (0.25 mM) for 30 min. Cells were fixed in 4% paraformaldehyde and
868 permeabilized in 0.1% Triton X-100. Immunofluorescence was performed for Hedls (PBs,
869 white) and DAPI (nuclei, blue). Scale bar=20 µm. C: HUVECs were transduced with
870 recombinant lentiviruses expressing either shRNAs targeting Atg5 (shAtg5) or a non-targeting
871 control (NS) and selected with puromycin (1 µg/mL). Cells were treated with Torin (250 nM) or
872 DMSO for 2 h prior to fixation in in 4% paraformaldehyde and permeabilization in 0.1% Triton
873 X-100. Samples were immunostained for the PB-resident protein Hedls (white) and nuclei
874 (DAPI). Scale bar=20 µm. Hedls puncta were quantified using CellProfiler and normalized to
875 the number of nuclei, results were plotted in GraphPad and a 2-way ANOVA was performed
876 with a Šidák's multiple comparison test, ±SEM; n=4, *=P<0.05.

877 **Figure 3: KapB-mediated ARE-mRNA reporter expression requires canonical autophagy.**
878 A: HUVECs were transduced with recombinant lentiviruses expressing either KapB or an empty
879 vector control and selected with blasticidin (5 µg/mL). Conditioned media harvested from
880 KSHV latently infected cells was used to mimic the KS lesion microenvironment and induce the
881 transcription of cytokines for 6 h prior to lysis for total RNA, normal media was used for the 0 h
882 time point. Transcript levels were quantified by qPCR and normalized to 18S as a reference
883 gene. Data is represented as the fold change in target transcript expression relative to the
884 untreated vector control and was quantified using the ΔΔCq method. Results were plotted in
885 GraphPad, a 2-way ANOVA was performed, ±SEM; n=3, *=P<0.05, **=P<0.01. B: HUVECs
886 were treated with Torin (250 nM) or a DMSO control for 2 h prior to lysis for total RNA.
887 Transcript levels were quantified by qPCR and normalized to HPRT as a reference gene. Data is
888 represented as the fold change in target transcript expression relative to the untreated vector
889 control and was quantified using the ΔΔCq method. An unpaired t-test was performed, ±SEM;
890 n=3, *=P<0.05. C: HeLa Tet-Off cells were co-transfected with expression plasmids for an
891 ARE-containing firefly luciferase plasmid (pTRE-Fluc-ARE) and a stable renilla luciferase
892 plasmid (pTRE-Rluc). 36 h post transfection, doxycycline (Dox) was added to halt reporter gene
893 transcription of both luciferase reporters, at the same time Torin (250 nM) or DMSO were added;
894 12 h after Dox addition, lysates were harvested in passive lysis buffer (Promega). Luciferase
895 activity for both firefly and renilla was analyzed using the Dual-Luciferase Reporter Assay
896 (Promega) and normalized (firefly/renilla) relative luciferase was calculated in relative light units
897 (RLUs). Results were plotted using GraphPad, an unpaired t-test was performed, ±SEM; n=6,
898 ***=P<0.001. D&E: HeLa Tet-Off cells were transduced with recombinant lentiviruses
899 expressing either shRNAs targeting Atg5 or Atg14 (shAtg5, shAtg14) or a non-targeting control

900 (NS) and selected with puromycin (1 µg/mL). After selection, cells were co-transfected and Dox
901 treatment was performed as described in C, except that co-transfection also included an
902 expression plasmid for KapB or an empty vector control. Results were plotted using GraphPad,
903 an unpaired t-test was performed, ±SEM; n=3, *=P<0.05, **=P<0.01. F: Cells were co-
904 transfected as in E and bafilomycin (10 nM) was added at the same time as Dox. Results were
905 plotted in GraphPad and a Student's t-test was performed, ±SEM; n=3, *=P<0.05, **=P<0.01.

906 **Figure 4: Dcp1a protein levels are decreased by KapB expression and Torin treatment.** A:
907 HUVECs were treated with DMSO or Torin (250 nM) for 4 h prior to harvest. Samples were
908 lysed in 2x Laemmli buffer and resolved by SDS-PAGE before immunoblotting with Xrn1,
909 EDC4/Hedls, Dcp1a, and DDX6. Samples were quantified by normalizing the PB resident
910 protein levels to the total protein in each lane and then the DMSO control using ImageLab
911 (Biorad). Results were plotted in GraphPad and a one-way ANOVA was performed ±SEM; n=3,
912 **=P<0.01. B: HUVECs were transduced with recombinant lentiviruses expressing either KapB
913 or an empty vector control and selected with blasticidin (5 µg/mL). Cells were treated with
914 DMSO or bafilomycin A1 (BafA1, 10 nM) for 4 h prior to harvest in 2x Laemmli buffer.
915 Samples were resolved by SDS-PAGE and immunoblot was performed for Dcp1a or p62
916 (autophagy marker). Samples were quantified by normalizing Dcp1a protein levels to the total
917 protein in each lane using Image Lab (Biorad) and then to the Vector DMSO control. Results
918 were plotted in GraphPad and a 2-way ANOVA was performed, ±SEM; n=3, ***=P<0.001. C:
919 HUVECs were transduced with recombinant lentiviruses expressing either KapB or an empty
920 vector control and selected with blasticidin (5 µg/mL). Samples were harvested in 2x Laemmli
921 buffer, resolved by SDS-PAGE and immunoblot was performed for Xrn1, Hedls/EDC4, or
922 DDX6. Samples were quantified by normalizing Dcp1a protein levels to the total protein in each

923 lane using Image Lab (Biorad) and then to the Vector DMSO control. Results were plotted in
924 GraphPad. D: HUVECs were sequentially transduced: first with recombinant lentiviruses
925 expressing either shRNAs targeting Atg5 (shAtg5) or a non-targeting control (NS) and selected
926 with puromycin (1 µg/mL), and second with either KapB or an empty vector control and selected
927 with blasticidin (5 µg/mL). Samples were harvested in 2x Laemmli buffer and resolved by SDS-
928 PAGE. Immunoblot was performed for Dcp1a, Atg5, and KapB. Samples were quantified by
929 normalizing Dcp1a protein levels to the total protein in each lange using Image Lab (Biorad) and
930 then to the Vector NS control. Results were plotted in GraphPad and a 2-way ANOVA was
931 performed, ±SEM; n=3, *=P<0.05, **P=<0.01.

932 **Figure 5. KapB-mediated PB disassembly and ARE-mRNA reporter expression require the**
933 **selective autophagy receptor NDP52**. A: HUVECs were sequentially transduced with
934 recombinant lentivirus expressing KapB or an empty vector control and selected with blasticidin
935 (5 µg/mL), and second with shRNAs targeting NDP52, OPTN, p62 or a non-targeting control
936 (NS) and selected with puromycin (1 µg/mL). Coverslips were fixed in 4% paraformaldehyde,
937 permeabilized in 0.1% Triton X-100 and immunostained for Hedls (PBs; white), DAPI (nuclei,
938 blue). Scale bar=20 µm. Cells were imaged and the mean number of Hedls puncta per cell were
939 quantified using CellProfiler. Data were plotted in GraphPad as the mean number of Hedls
940 puncta per cell per condition ± SEM; n=3. A 2-way ANOVA was performed with a Šidák's
941 multiple comparison test; * = P<0.05 **= P<0.01. B: HUVECs were transduced with
942 recombinant lentivirus expressing an shRNA targeting NDP52 and selected with puromycin (1
943 µg/mL). Cells were treated with Torin (250 nM) or a DMSO control for 2 h prior to fixation in
944 4% paraformaldehyde and permeabilization in 0.1% Triton X-100. Samples were
945 immunostained for Hedls (PBs; white), DAPI (nuclei, blue). Scale bar=20 µm. Cells were

946 imaged and the mean number of Hedls puncta per cell were quantified using CellProfiler. Data
947 were plotted in GraphPad as the mean number of Hedls puncta per cell per condition. Results
948 were plotted in GraphPad, a 2-way ANOVA was performed with a Šidák's multiple comparison
949 test, ± SEM; n=3. * = P<0.05. C: HeLa Tet-Off cells were transduced with recombinant
950 lentivirus expressing shRNAs targeting NDP52, OPTN, p62 or a NS control and selected with
951 puromycin (1μg/mL) then cells were co-transfected, treated with Dox and luciferase activity was
952 recorded and analyzed as in Figure 3. Data were plotted in GraphPad as the mean fold change in
953 the relative luciferase activity of each condition compared to vector NS or KapB NS; n=3. An
954 unpaired t-test was performed; * = P<0.05 **= P<0.01. D: Schematic of NDP52. NDP52
955 contains the following domains and interacting regions: SKICH domain (SKIP-carboxyl
956 homology domain), CLIR (non-canonical LC3-interaction motif), coiled-coil domain, GALB
957 (galectin binding domain) ZF1 & ZF2 (zinc finger domains). Known mutations that disrupt
958 NDP52 function include: V136S which prevents binding to LC3-C and C443K which prevents
959 binding to ubiquitin. E: HUVECs were sequentially transduced first with recombinant lentivirus
960 expressing shDNP52 targeting the 3'-UTR of NDP52 or a NS control and selected with
961 blasticidin (5 μg/mL), and second, with KapB and one of the following: mCherry control (mCh),
962 RFP-NDP52 wt, mCh-NDP52 C443K or mCh-NDP52 V136S/C443K. Coverslips were fixed
963 with 4% paraformaldehyde, permeabilized with 0.1% Triton X-100, and immunostained with
964 Hedls (PBs, green). Scale bar=20 μm. F: Samples from E were quantified; Hedls puncta were
965 counted using CellProfiler and normalized to the number of nuclei, results were plotted in
966 GraphPad, a 2-way ANOVA was performed with a Šidák's multiple comparison test, ± SEM;
967 n=3. * = P<0.05, **=P<0.01.

968 **Figure 6: MK2EE-mediated PB disassembly does not require NDP52 or canonical**
969 **autophagy.** A: HUVECs were transduced with recombinant lentiviruses expressing either
970 constitutively active MK2 (MK2EE) or an empty vector control and selected with blasticidin (5
971 µg/mL) for 48 h. Cells were treated with DMSO or bafilomycin A1 (10 nM) for 30 min before
972 being fixed in methanol. Immunofluorescence was performed for LC3 (autophagosomes, white)
973 and DAPI (nuclei, blue). Scale bar=20 µm. Total LC3 area per field was quantified by
974 identifying LC3 puncta using CellProfiler and normalizing to the number of nuclei and the vector
975 DMSO control. Results were plotted in GraphPad and a 2-way ANOVA was performed with a
976 Šidák's multiple comparison test, ±SEM n=3; *=P<0.05. B: HUVECs were transduced with
977 recombinant lentiviruses expressing either MK2EE or an empty vector control and selected with
978 blasticidin (5 µg/mL). Cells were treated with bafilomycin A1 (10 nM) or a vehicle control
979 (DMSO) for the indicated times prior to harvest in 2x Laemmli buffer. Protein lysates were
980 resolved by SDS-PAGE and immunoblot was performed for p62 and LC3. Samples were
981 quantified using Image Lab (Biorad) software and then normalized, first to total protein and then
982 to their respective starting points (time 0 h). Results were plotted in GraphPad and a linear
983 regression statistical test was performed, ±SEM; n=3, *=P<0.05, **=P<0.01. C: HUVECs were
984 sequentially transduced: first with recombinant lentiviruses expressing either shRNAs targeting
985 Atg5 (shAtg5) or a non-targeting control (NS) and selected with puromycin (1 µg/mL), and
986 second, with either MK2EE or an empty vector control and selected with blasticidin (5 µg/mL).
987 Coverslips were fixed in 4% paraformaldehyde, permeabilized in 0.1% Triton X-100, and
988 immunostained for the PB-resident protein Hedls (PBs, white) and DAPI (nuclei, blue). Scale
989 bar=20 µm. Hedls puncta were counted using CellProfiler and normalized to the number of
990 nuclei, results were plotted in GraphPad and a 2-way ANOVA was performed with a Šidák's

991 multiple comparison test, ±SEM n=5; *=P<0.05. D: HeLa Tet-Off cells were transduced with
992 recombinant lentiviruses expressing either shRNAs targeting Atg5 (shAtg5) or a non-targeting
993 control (NS) and selected with puromycin (1 µg/mL) then co-transfected with expression
994 plasmids for pTRE-Fluc-ARE, pTRE-Rluc, and MK2EE or an empty vector control, and treated
995 as in Figure 3. Results were plotted using GraphPad, a Student's t-test was performed, ±SEM,
996 n=4; *=P<0.05. E: HUVECs were sequentially transduced with recombinant lentivirus
997 expressing shRNAs targeting NDP52, OPTN, p62 or a non-targeting control (NS) and selected
998 with puromycin (1 µg/mL) and second with recombinant lentivirus expressing constitutively
999 active MK2EE or an empty vector control and selected with blasticidin (5 µg/mL). Coverslips
1000 were fixed in 4% v/v paraformaldehyde, permeabilized in 0.1% Triton X-100, and
1001 immunostained for Hedls (PBs, white) and DAPI (nuclei, blue). Scale bar = 20 µm. Hedls puncta
1002 were counted using CellProfiler and normalized to the number of nuclei, results were plotted in
1003 GraphPad, ±SEM; n=3. F: HeLa Tet-Off cells were transduced with recombinant lentivirus
1004 expressing shRNAs targeting NDP52, OPTN, p62 or a NS control and selected with puromycin
1005 (1µg/mL) then cells were co-transfected, treated with Dox and luciferase activity was recorded
1006 and analyzed as in Figure 3. Data were plotted in GraphPad as the mean fold change in the
1007 relative luciferase activity of each condition compared to vector NS or MK2EE NS; n=3. An
1008 unpaired t-test was performed; * = P<0.05 **= P<0.01.

1009 **Figure 7: Model of NDP52-dependent PB disassembly elicited by KapB.** A: KapB expression
1010 has the potential to impact two pathways that lead to PB disassembly, thereby increasing the
1011 stability/translation of AU-rich containing inflammatory cytokine mRNA. The first pathway is
1012 dependent on canonical autophagy and the SAR, NDP52, and is also used to elicit PB
1013 disassembly by the mTOR inhibitor, Torin. Because of its ability to bind and activate MK2,

1014 KapB also may promote PB disassembly using an autophagy-independent pathway that relies on
1015 phosphorylated, active MK2, a pathway that is mimicked by overexpression of MK2EE. B:
1016 Under normal conditions, the cytoplasm of all cells contain PBs, granules comprised of RNA and
1017 RNA decay proteins that are visible by immunofluorescent microscopy. When KapB is
1018 expressed, microscopically visible PBs are lost but can reform after overexpression of Dcp1a-
1019 GFP or after stress-induced translation shutoff. PB disassembly elicited by KapB depends on the
1020 selective autophagy receptor, NDP52. KapB expression decreases the steady-state level of the
1021 PB protein, Dcp1a, but does not markedly alter the levels of other PB proteins like DDX6,
1022 ECD4/Hedls, or Xrn1. Dcp1a has been shown to be modified by phosphorylation and
1023 ubiquitination (Tenekeci *et al*, 2016; Aizer *et al*, 2013; Chiang *et al*, 2013) and these
1024 modifications alter PB formation and function. These data lead us to propose the following
1025 model. KapB expression leads to an as yet undetermined post-translational modification that
1026 promotes its recognition by the selective autophagy receptor, NDP52. Simultaneous binding of
1027 NDP52 to modified Dcp1a (or another unidentified PB protein) and to LC3 on the nascent
1028 phagophore recruit Dcp1a to the autophagosome for degradation. The loss of Dcp1a or another
1029 PB protein via selective autophagy leads to PB disassembly but does not prevent *de novo* PB
1030 assembly under stress, even during KapB expression.

1031 DDX6/Rck: RNA helicase, EDC4/Hedls: decapping co-factor, Dcp2: catalytic component of
1032 decapping machinery, Dcp1a: decapping co-factor, ECD3: decapping enhancer, Xrn1: 3'-5'
1033 exonuclease.

1034

1035

1036

1037 **Tables**

1038

1039 **Table 1: Drugs**

Drug	Vendor/Catalogue #	Concentration
Torin1	Sigma-Aldrich 475991	250 nM
Bafilomycin A1	Sigma-Aldrich B1793	10 nM
Chloroquine	Sigma-Aldrich C6628	25 µM
MG-132	Selleckchem S2619	5 µM
LPS	Sigma-Aldrich L3129	1 µg/mL
Sodium Arsenite	Sigma-Aldrich 1.06277	0.25 mM
Doxycycline	Sigma-Aldrich D9891	1 µg/mL

1040

1041 **Table 2: Plasmids**

Plasmid	Use	Source	Mammalian Selection
pBMN mCh NDP52 C443K	UBD mutant	Addgene #119685 (Padman et al., 2019)	N/A
pBMN mCh NDP52 C443K V136S	UBD/LIR mutant	Addgene #119686 (Padman et al., 2019)	N/A
RFP-NDP52	Overexpression	Dr. Andreas Till (University Hospital of Bonn)	N/A
pcDNA 3.1 (+)	Empty Vector Control	Invitrogen V79020	N/A
pcDNA KapB BCBL1	ARE-mRNA stability	(Corcoran et al., 2015)	N/A
pcDNA FLAG-MK2EE	ARE-mRNA stability	(Corcoran et al., 2015)	N/A
pLKO.1-TRC	shRNA expression	Addgene #10878 (Moffat et al., 2006)	Puromycin
pLKO.1-blast	shRNA expression	Addgene #26655 (Bryant et al., 2010)	Blasticidin
pLJM1	Empty Vector Control	(Johnston et al., 2019)	Blasticidin/ Puromycin
pLJM1 KapB (pulmonary KS)	Overexpression	Cloned from pBMNIP-KapB (Corcoran et al., 2015) into pLJM1-BSD	Blasticidin

Plasmid	Use	Source	Mammalian Selection
pLJM1 mCh	Overexpression Control	Craig McCormick (Dalhousie University)	Blasticidin
pLJM1 FLAG-MK2EE	Overexpression	Cloned into pLJM1 using BamHI and EcoRI from pBMN FLAG-MK2EE (Corcoran et al., 2015)	Blasticidin/ Puromycin
pLJM1 RFP-NDP52	Overexpression	Cloned into pLJM1 using NheI and BamHI from RFP-NDP52	Puromycin
pLJM1 mCh-NDP52 C443K	Overexpression	Cloned into pLJM1 from Addgene #119685 using the primers listed in Table 4	Blasticidin/ Puromycin
pLJM1 mCh-NDP52 C443K V136S	Overexpression	Cloned into pLJM1 from Addgene #119686 using the primers listed in Table 4	Blasticidin/ Puromycin
pMD2.G	Lentivirus generation	Addgene #12259	N/A
psPAX2	Lentivirus generation	Addgene #12260	N/A
pTRE2 Firefly Luciferase-ARE	ARE-mRNA stability	(Corcoran et al., 2011)	N/A
pTRE2-Renilla Luciferase	ARE-mRNA stability	(Corcoran et al., 2011)	N/A

1042

1043 **Table 3: shRNA target sequences**

shRNA target	shRNA sequence 5'→3'	Region
Non-targeting (NS)	AGCACAAGCTGGAGTACAACTA	
Atg5	CTTTGATAATGAACAGTGAGA	CDS
NDP52(1)	GAGCTGCTTCAACTGAAAGAA	CDS
NDP52(2)	GACTTGCCTATGGAAACCCAT	CDS
NDP52(3)	CCCTTTGTGAACTAAGTTCAA	3'-UTR
NDP52(4)	CCTGACTTGATACTAAGTGAT	3'-UTR
Optineurin (1)	GCACGGCATTGTCTAAATATA	CDS
Optineurin (2)	GCCATGAAGCTAAATAATCAA	CDS
p62	CCGAATCTACATTAAAGAGAA	CDS
NBR1 (1)	GCCAGGAACCAAGTTTATCAA	CDS
NBR1 (2)	CCATCCTACAATATCTGTGAA	CDS
VCP (1)	ACCGTCCCAATCGGTTAATTG	CDS
VCP (2)	AGATCCGTCGAGATCACTTTG	CDS

1044

1045 **Table 4: Cloning primers**

Primer	Primer Sequence

NDP52 C443K & C443K/V136S BamHI-Forward	5' TAAGCAGGATCCGCCACCATGGTGAGCAAG 3'
NDP52 C443K & C443K/V136S EcoRI-Reverse	5' TAAGCAGAATTCCAGAGAGAGTGTTTGAACACGT 3'

1046

1047 **Table 5: Antibodies**

Antibody	Species	Vendor/Catalogue #	Application	Dilution
Hedls	Mouse	Santa Cruz sc-8418	Immunofluorescence Immunoblot	1:1000 1:1000
KapB	Rabbit	A generous gift from Don Ganem	Immunofluorescence	1:1000
NDP52	Rabbit	CST 60732	Immunoblot	1:1000
p62	Rabbit	CST 7695	Immunoblot	1:1000
Dcp1a	Mouse	CST 15365	Immunoblot	1:500
DDX6	Rabbit	Bethyl A300-461	Immunoblot	1:1000
MK2	Rabbit	CST 12155	Immunofluorescence	1:1000
LC3B	Rabbit	CST 2775	Immunofluorescence Immunoblot	1:200 1:1000
Atg5	Rabbit	CST 2630	Immunoblot	1:1000
Atg14	Rabbit	CST 96752	Immunoblot	1:1000
OPTN	Rabbit	Abcam ab23666	Immunoblot	1:1000
Xrn1	Rabbit	Abcam ab231197	Immunoblot	1:1000
VCP	Rabbit	CST 2649	Immunoblot	1:1000
NBR1	Rabbit	CST 9891	Immunoblot	1:1000

1048

1049 **Table 6: qPCR primers**

Primer	Primer Sequence
HPRT-1- Forward	5’ CTTTCCTTGGTCAGGCAGTATAA 3’
HPRT-2 - Reverse	5’ AGTCTGGCTTATATCCAACACTTC 3’
18S - Forward	5’ TTCGAACGTCTGCCCTATCAA 3’
18S - Reverse	5’ GATGTGGTAGCCGTTTCTCAGG 3’
IL-6 - Forward	5’ GAAGCTCTATCTCGCCTCCA 3’
IL-6 - Reverse	5’ TTTTCTGCCAGTGCCTCTTT 3’
CXCL8 - Forward	5’ AAATCTGGCAACCCTAGTCTG 3’
CXCL8 - Reverse	5’ GTGAGGTAAGATGGTGGCTAAT 3’
IL-1β - Forward	5’ CTCTCACCTCTCCTACTCACTT 3’
IL-1β - Reverse	5’ TCAGAATGTGGGAGCGAATG 3’
COX-2 - Forward	5’ CCCTTGGGTGTCAAAGGTAA 3’
COX-2 - Reverse	5’ GCCCTCGCTTATGATCTGTC 3’

1050

1051

1052

1053

1054 **Supplemental Figure Legends**

1055 **Figure S1: KapB expression promotes PB disassembly but does not prevent PB assembly.**
1056 HeLa cells expressing a doxycycline-inducible GFP-Dcp1a were used to determine whether
1057 KapB prevented granule assembly or promoted disassembly. A: HeLa cells were transfected
1058 with either KapB or an empty vector control prior to inducing expression of GFP-Dcp1a with
1059 doxycycline (1 µg/mL). Cells were fixed 12 h post-induction and immunostained for Hedls
1060 (PBs, red) and KapB (blue). Scale bar=20 µm. B: GFP-Dcp1a expression was induced with
1061 doxycycline (1 µg/mL) in HeLa cells prior to transfection with either KapB or an empty vector
1062 control. Cells were fixed 12 h post-transfection and immunostained for Hedls (PBs, red) and
1063 KapB (blue). Scale bar=20 µm. C: HUVECs were transduced with recombinant lentiviruses
1064 expressing either Kaposin B (KapB) or an empty vector control and selected with blasticidin (5
1065 µg/mL). Cells were treated with sodium arsenite (0.25 mM) or a vehicle control for 30 min prior
1066 to fixation in 4% paraformaldehyde and permeabilization in 0.1% Triton X-100. Scale bar=20
1067 µm.

1068

1069 **Figure S2: Canonical autophagy knockdown prevents KapB-mediated PB disassembly.**
1070 A&B: HUVECs were sequentially transduced: first with recombinant lentiviruses expressing
1071 either shRNAs targeting Atg5 or Atg14 (shAtg5, shAtg14) or a non-targeting control (NS) and
1072 selected with puromycin (1 µg/mL), and second with either KapB or an empty vector control and
1073 selected with blasticidin (5 µg/mL). Samples were lysed in 2x Laemmli and resolved by SDS-
1074 PAGE. Samples were immunoblotted for Atg5 (A) or Atg14 (B). For Atg5 (A) samples were
1075 quantified by normalizing Atg5 protein levels to the total protein in each lane using Image Lab
1076 (Biorad) and then to Vector NS. Results were plotted in GraphPad, a 2-way ANOVA was

1077 performed, ±SEM; n=3, ***=P<0.001. C: Atg5 +/+ (WT) and -/- (KO) MEFs were transduced as
1078 in A and harvested in 2x Laemmli buffer before being resolved by SDS-PAGE. Samples were
1079 probed for LC3, a representative blot is shown. D: Atg5 +/+ and -/- MEFs were transduced with
1080 recombinant viruses expressing KapB or an empty vector control and selected with blasticidin (5
1081 µg/mL). Samples were fixed in 4% paraformaldehyde and permeabilized in 0.1% Triton X-100.
1082 Immunofluorescence was performed for Hedls (PBs, white) and DAPI (nuclei, blue). Scale
1083 bar=20 µm. Hedls puncta were counted using CellProfiler and normalized to the number of
1084 nuclei, results were plotted in GraphPad and a 2-way ANOVA was performed with a Šidák's
1085 multiple comparison test, ±SEM; n=3, *=P<0.05, **=P<0.01.

1086 **Figure S3: Canonical autophagy shRNA silencing in HeLa cells.** A&B: HeLas were
1087 transduced with recombinant lentiviruses expressing either shRNAs targeting Atg5 or Atg14
1088 (shAtg5, shAtg14) or a non-targeting control (NS) and selected with puromycin (1 µg/mL) prior
1089 to transfection with KapB or an empty vector for luciferase assays. Samples were lysed in 2x
1090 Laemmli buffer and resolved by SDS-PAGE before immunoblotting with Atg5 (A) or Atg14 (B).
1091 Representative blots are shown.

1092 **Figure S4: Selective autophagy receptor knockdown in HUVECs reveals that OPTN and**
1093 **p62 are not required for KapB-mediated PB disassembly.** A&B: HUVECs were transduced
1094 with shRNAs targeting VCP, NBR1, or a non-targeting control (NS) and selected with
1095 puromycin (1 µg/mL), then transduced with an empty vector control or KapB and selected with
1096 blasticidin (5 µg/mL). Samples were lysed in 2x Laemmli buffer, resolved by SDS-PAGE, and
1097 immunoblotted for NBR1 (A) and VCP (B). Representative blots are shown, successful VCP
1098 knockdown was lethal, while NBR1 knockdown was not successful. C: HUVECs were
1099 transduced with shRNAs targeting NDP52 or a non-targeting control (NS) and selected with

1100 puromycin (1 µg/mL), then transduced with an empty vector control or KapB and selected with
1101 blasticidin (5 µg/mL). Samples were lysed in 2x Laemmli buffer, resolved by SDS-PAGE, and
1102 immunoblotted for NDP52. D&E: HUVECs were transduced with shRNAs targeting p62,
1103 OPTN, or a non-targeting control (NS) and selected with puromycin (1 µg/mL), then transduced
1104 with an empty vector control or KapB and selected with blasticidin (5 µg/mL). Samples were
1105 lysed in 2x Laemmli buffer and resolved by SDS-PAGE. Samples were immunoblotted for p62
1106 (D) and OPTN (E), representative blots are shown. F: HUVECs were transduced as in D and E.
1107 Coverslips were fixed in 4% paraformaldehyde, permeabilized in 0.1% Triton X-100 and
1108 immunostained for Hedls (PBs; white), DAPI (nuclei, blue). Scale bar=20 µm. G: HUVECs were
1109 transduced with recombinant lentiviruses targeting NDP52 or a non-targeting control (NS) and
1110 selected with puromycin (1 µg/mL). Samples were lysed in 2x Laemmli buffer, resolved by
1111 SDS-PAGE, and immunoblotted for NDP52 to confirm knockdown for paired Torin
1112 immunofluorescence experiments.

1113

1114 **Figure S5: shRNA silencing of selective autophagy receptors in HeLa cells.** A, B&C: HeLas
1115 were transduced with shRNAs targeting NDP52, OPTN, p62, or a non-targeting control (NS) and
1116 selected with puromycin (1 µg/mL) prior to transfection with KapB or an empty vector for
1117 luciferase assays. Samples were lysed in 2x Laemmli buffer, resolved by SDS-PAGE, and
1118 immunoblotted for NDP52 (A), p62 (B), and OPTN (C). Representative blots are shown.

1119

1120 **Figure S6: NDP52 shRNA silencing and rescue in control HUVECs.** A: Representative
1121 western blot of HUVECs transduced with an shRNA targeting the 3'UTR of NDP52 or a non-

1122 targeting control (NS) and selected with puromycin (1 µg/mL), then co-transduced with an
1123 empty vector control and mCherry (mCh) or KapB and mCh. Samples were lysed in 2x
1124 Laemmli, resolved by SDS-PAGE, and immunoblotted for NDP52. B: HUVECs were
1125 sequentially transduced first with recombinant lentivirus expressing shDNP52 targeting the 3'-
1126 UTR of NDP52 or a NS control and selected with blasticidin (5 µg/mL), and second, with vector
1127 and one of the following: mCherry control (mCh), RFP-NDP52 wt, mCh-NDP52 C443K or
1128 mCh-NDP52 V136S/C443K. Coverslips were fixed with 4% v/v paraformaldehyde,
1129 permeabilized with 0.1% Triton X-100, and were immunostained with Hedls (PBs, green). Scale
1130 bar=20 µm. C: Hedls puncta were counted using CellProfiler and normalized to the number of
1131 nuclei, results were plotted in GraphPad.

1132 **Figure S7: shRNA silencing of canonical and selective autophagy genes in MK2EE-**
1133 **expressing cells.** A: HUVECs were transduced with shRNAs targeting Atg5 or a non-targeting
1134 control (NS) and selected with puromycin (1 µg/mL), then transduced with an empty vector
1135 control or KapB and selected with blasticidin (5 µg/mL). Samples were lysed in 2x Laemmli
1136 buffer, resolved by SDS-PAGE, and immunoblotted for Atg5. A representative blot is shown. B:
1137 HeLas were transduced with recombinant lentiviruses expressing either shRNAs targeting Atg5
1138 or a non-targeting control (NS) and selected with puromycin (1 µg/mL) prior to transfection with
1139 MK2EE or an empty vector for luciferase assays. Samples were lysed in 2x Laemmli buffer and
1140 resolved by SDS-PAGE before immunoblotting for Atg5. A representative blot is shown. C,
1141 D&E: HUVECs were transduced with shRNAs targeting NDP52, p62, OPTN, or a non-targeting
1142 control (NS) and selected with puromycin (1 µg/mL), then transduced with an empty vector
1143 control or MK2EE and selected with blasticidin (5 µg/mL). Samples were lysed in 2x Laemmli
1144 buffer and resolved by SDS-PAGE. Samples were immunoblotted for NDP52 (C), p62 (D), and

1145 OPTN (E), representative blots are shown. F: HUVECs were transduced with shRNAs as in
1146 D&E. Coverslips were fixed, permeabilized, and immunostained for Hedls (PBs; white), DAPI
1147 (nuclei, blue). Scale bar=20 µm. G, H&I: HeLas were transduced with shRNAs targeting
1148 NDP52, OPTN, p62, or a non-targeting control (NS) and selected with puromycin (1 µg/mL),
1149 then transfected with an empty vector control or MK2EE for luciferase assays. Samples were
1150 lysed in 2x Laemmli buffer, resolved by SDS-PAGE, and immunoblotted for NDP52 (G), p62
1151 (H), and OPTN (I). Representative blots are shown.

1152

1153

Figure 1

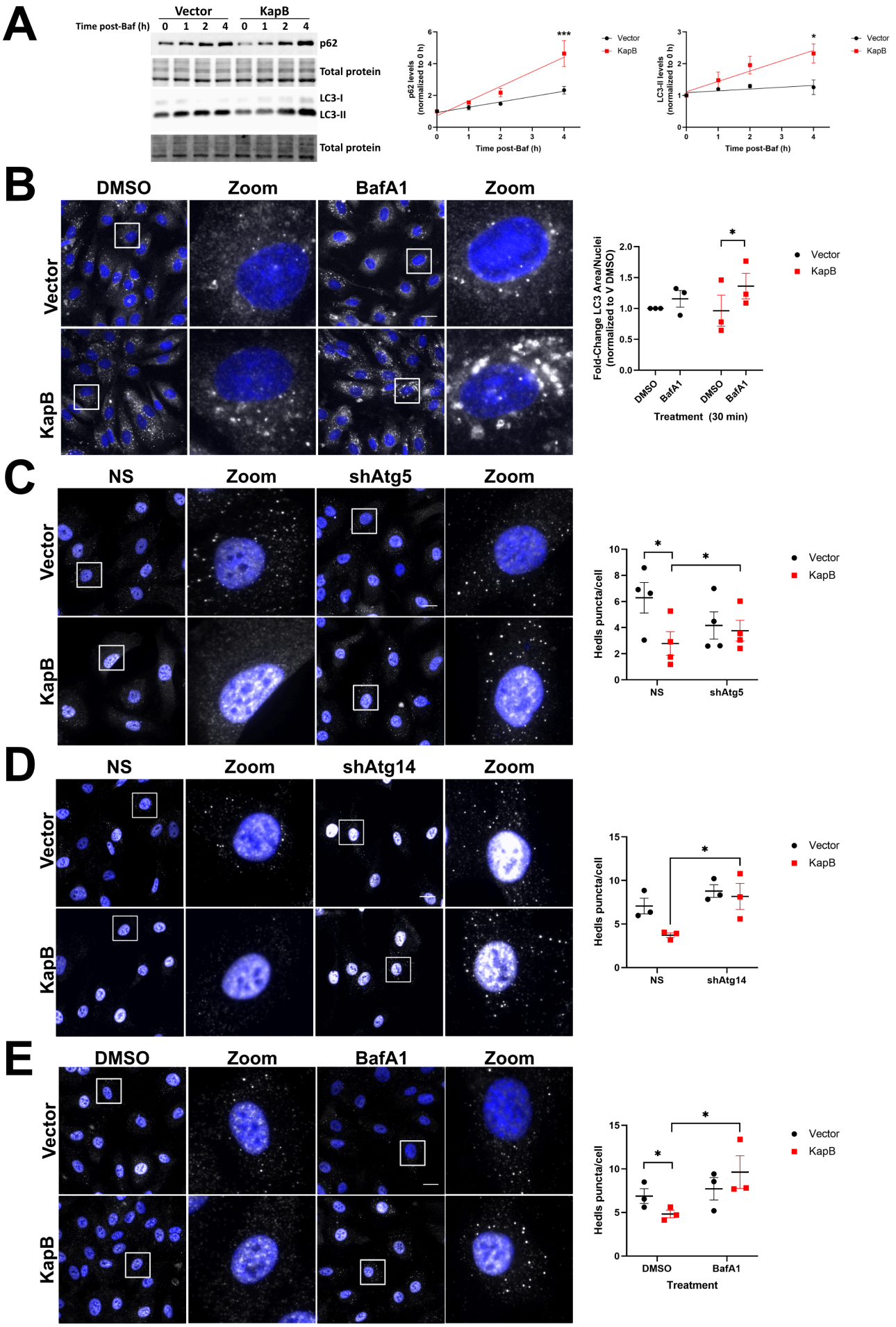
A
Vector
KapB
Time post-Baf (h)
0 1 2 4 0 1 2 4
p62
Total protein
LC3-I
LC3-II
Total protein
p62 levels (normalized to 0 h)
Time post-Baf (h)
***
LC3-II levels (normalized to 0 h)
*
Vector
KapB
B
DMSO
Zoom
BafA1
Zoom
Vector
KapB
Fold-Change LC3 Area/Nuclei (normalized to V DMSO)
Treatment (30 min)
DMSO
BafA1
C
NS
Zoom
shAtg5
Zoom
Hedls puncta/cell
D
NS
Zoom
shAtg14
Zoom
E
DMSO
Zoom
BafA1
Zoom
Treatment

Figure 2

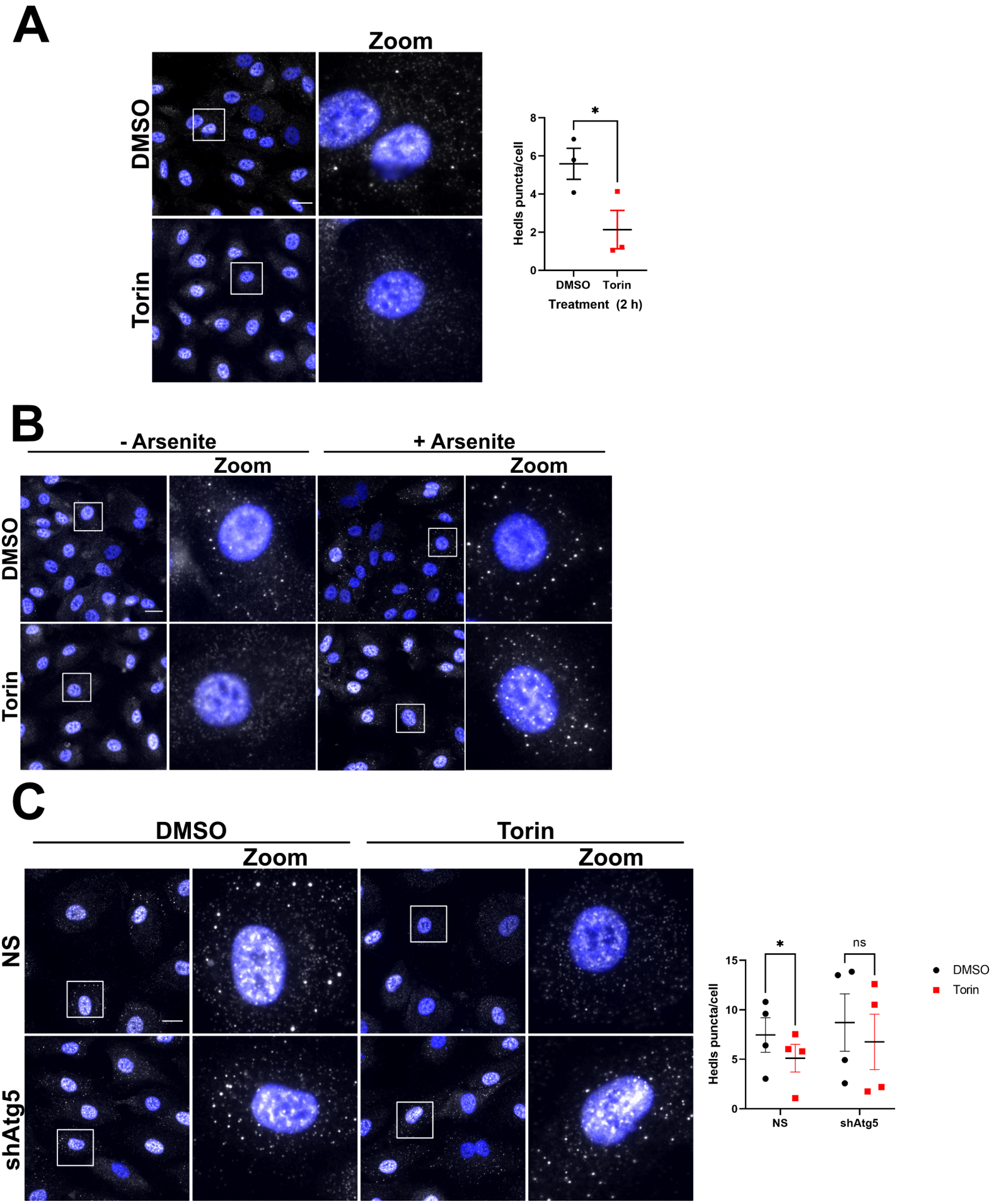
A
Zoom
DMSO
Torin
Hedls puncta/cell
8
6
4
2
0
*
DMSO
Torin
Treatment (2 h)
B
- Arsenite
+ Arsenite
Zoom
Zoom
DMSO
Torin
C
DMSO
Torin
Zoom
Zoom
NS
shAtg5
Hedls puncta/cell
15
10
5
0
*
ns
NS
shAtg5
DMSO
Torin

Figure 3

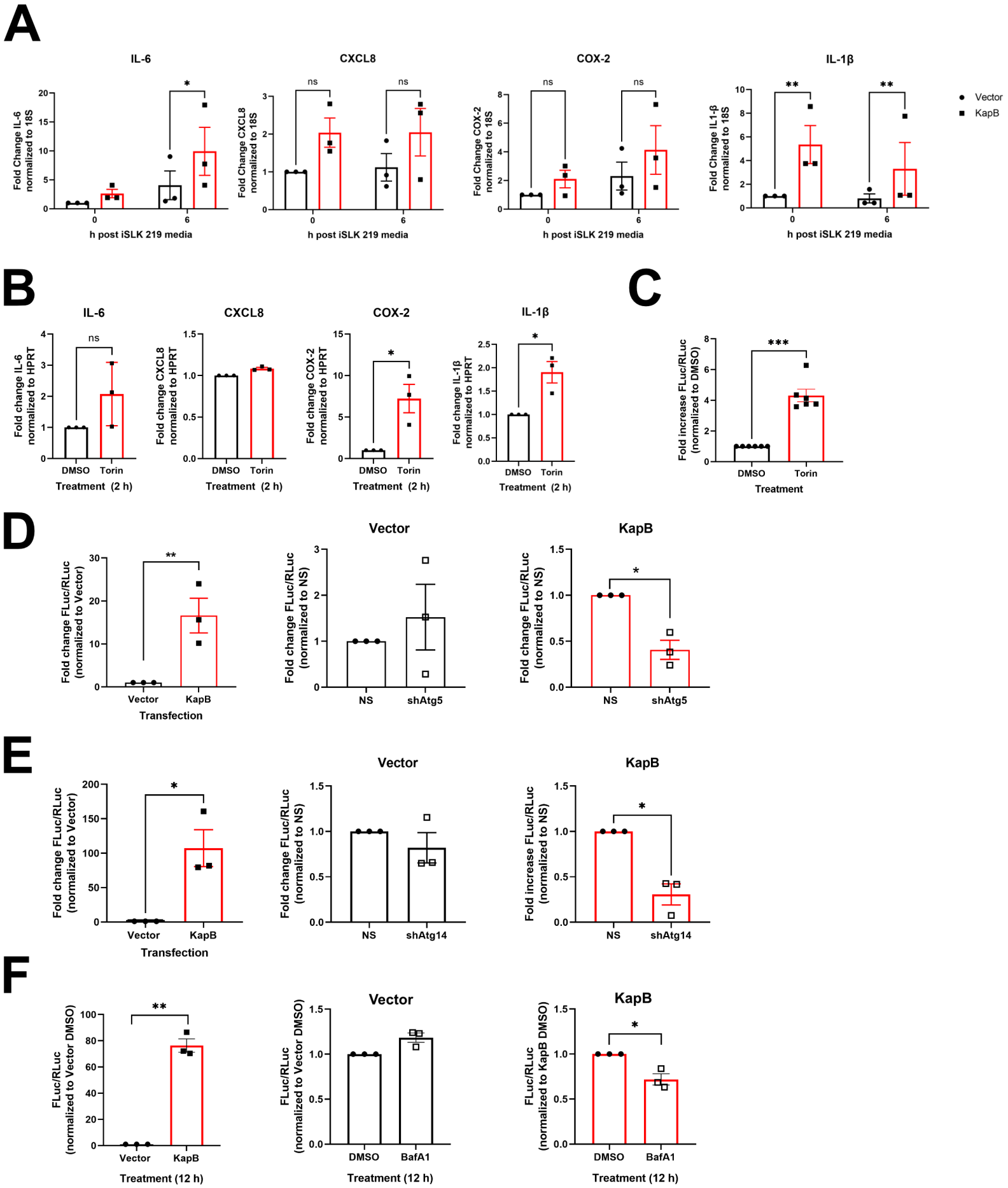
A
IL-6
CXCL8
COX-2
IL-1β
Fold Change IL-6 normalized to 18S
Fold Change CXCL8 normalized to 18S
Fold Change COX-2 normalized to 18S
Fold Change IL1-β normalized to 18S
h post iSLK 219 media
Vector
KapB
B
Fold change IL-6 normalized to HPRT
Fold change CXCL8 normalized to HPRT
Fold change COX-2 normalized to HPRT
Fold change IL-1β normalized to HPRT
DMSO
Torin
Treatment (2 h)
C
Fold increase FLuc/RLuc (normalized to DMSO)
Treatment
D
Fold change FLuc/RLuc (normalized to Vector)
Transfection
Fold change FLuc/RLuc (normalized to NS)
NS
shAtg5
E
Fold increase FLuc/RLuc (normalized to NS)
shAtg14
F
FLuc/RLuc (normalized to Vector DMSO)
FLuc/RLuc (normalized to KapB DMSO)
BafA1
Treatment (12 h)

Figure 4

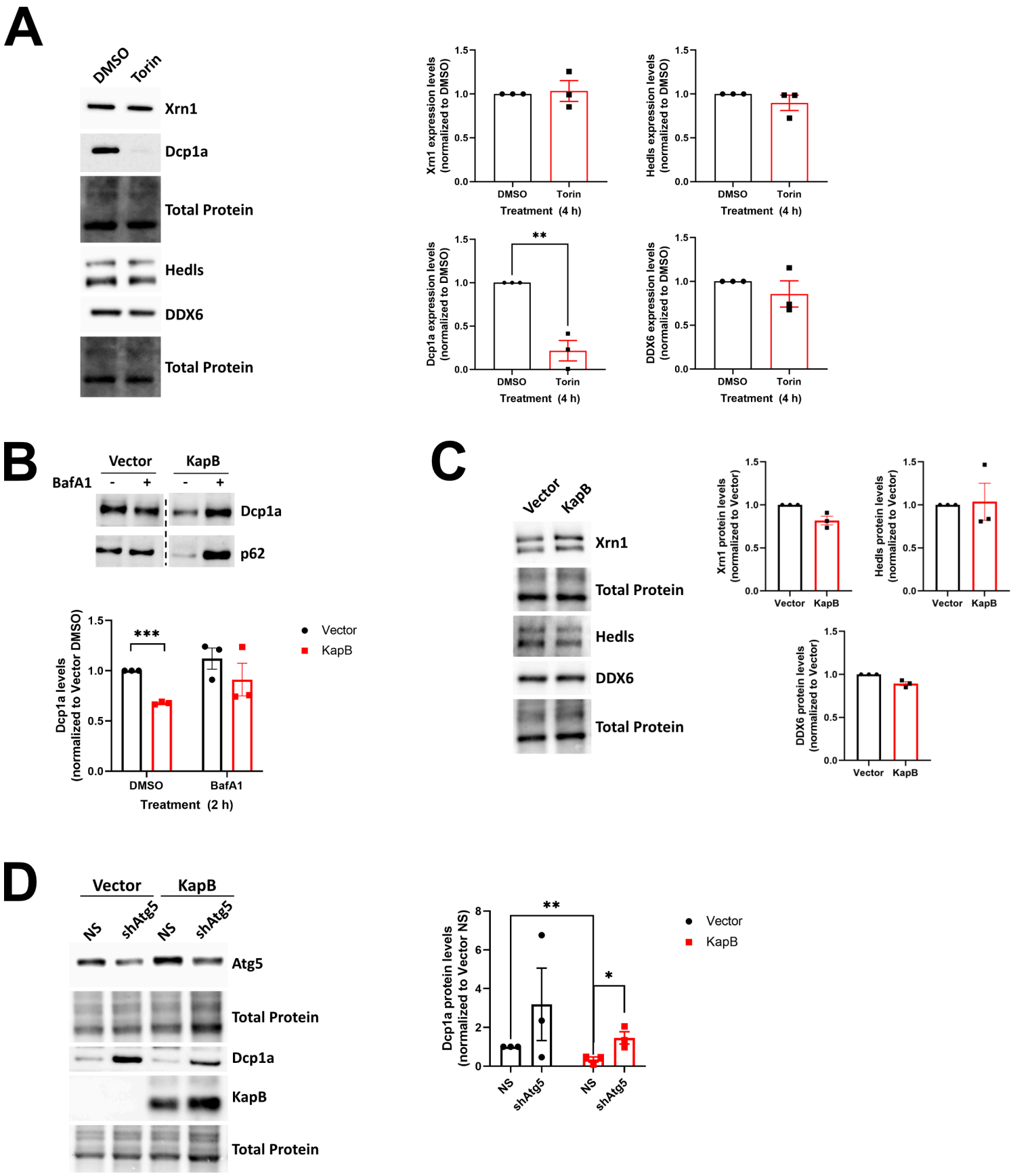
A
DMSO
Torin
Xrn1
Dcp1a
Total Protein
Hedls
DDX6
Total Protein
Xrn1 expression levels (normalized to DMSO)
Hedls expression levels (normalized to DMSO)
Dcp1a expression levels (normalized to DMSO)
DDX6 expression levels (normalized to DMSO)
Treatment (4 h)
**
B
Vector
KapB
BafA1
Dcp1a
p62
Dcp1a levels (normalized to Vector DMSO)
***
DMSO
BafA1
Treatment (2 h)
Vector
KapB
C
Vector
KapB
Xrn1
Total Protein
Hedls
DDX6
Total Protein
Xrn1 protein levels (normalized to Vector)
Hedls protein levels (normalized to Vector)
DDX6 protein levels (normalized to Vector)
D
Vector
KapB
NS
shAtg5
Atg5
Total Protein
Dcp1a
KapB
Total Protein
Dcp1a protein levels (normalized to Vector NS)
**
*

Figure 5

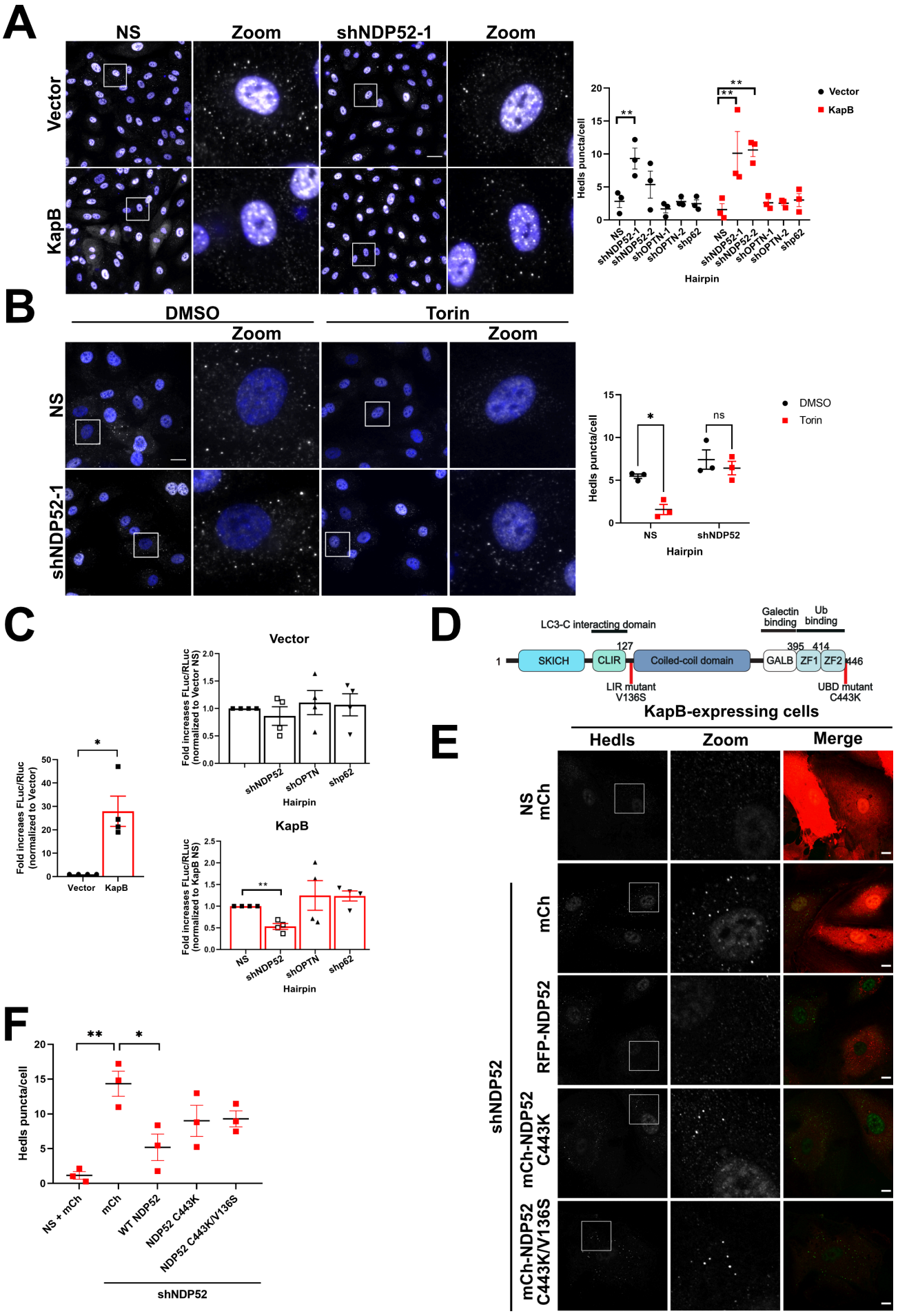
A
NS
Zoom
shNDP52-1
Zoom
Vector
KapB
Hedls puncta/cell
Vector
KapB
NS
shNDP52-1
shNDP52-2
shOPTN-1
shOPTN-2
shp62
Hairpin
B
DMSO
Torin
Zoom
Zoom
NS
shNDP52-1
Hedls puncta/cell
DMSO
Torin
ns
NS
shNDP52
Hairpin
C
Fold increaes FLuc/Rluc (normalized to Vector)
Vector
KapB
Vector
Fold increases FLuc/RLuc (normalized to Vector NS)
shNDP52
shOPTN
shp62
Hairpin
KapB
Fold increases FLuc/RLuc (normalized to KapB NS)
NS
shNDP52
shOPTN
shp62
Hairpin
D
LC3-C interacting domain
Galectin binding
Ub binding
127
395
414
1
SKICH
CLIR
Coiled-coil domain
GALB
ZF1
ZF2
446
LIR mutant V136S
UBD mutant C443K
E
KapB-expressing cells
Hedls
Zoom
Merge
NS mCh
mCh
RFP-NDP52
mCh-NDP52 C443K
mCh-NDP52 C443K/V136S
shNDP52
F
Hedls puncta/cell
NS + mCh
mCh
WT NDP52
NDP52 C443K
NDP52 C443K/V136S
shNDP52

Figure 6

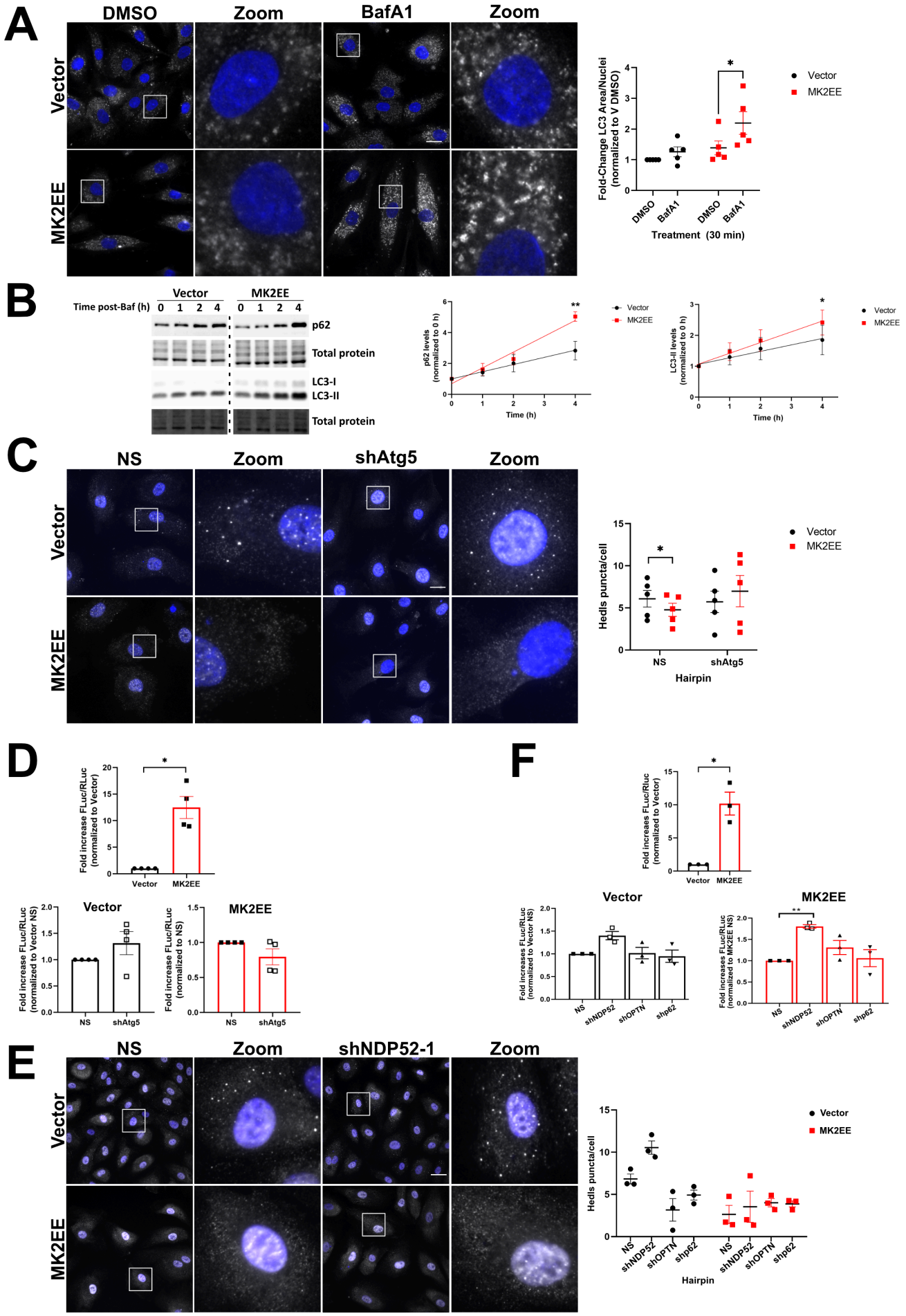
A
DMSO
Zoom
BafA1
Zoom
Vector
MK2EE
Fold-Change LC3 Area/Nuclei (normalized to V DMSO)
Vector
MK2EE
DMSO
BafA1
DMSO
BafA1
Treatment (30 min)
B
Vector
MK2EE
Time post-Baf (h)
0 1 2 4
0 1 2 4
p62
Total protein
LC3-I
LC3-II
Total protein
p62 levels (normalized to 0 h)
Time (h)
LC3-II levels (normalized to 0 h)
Time (h)
C
NS
Zoom
shAtg5
Zoom
Vector
MK2EE
Hedls puncta/cell
NS
shAtg5
Hairpin
D
Fold increase FLuc/RLuc (normalized to Vector)
Vector
MK2EE
Vector
MK2EE
Fold increase FLuc/RLuc (normalized to Vector NS)
Fold increase FLuc/RLuc (normalized to NS)
NS
shAtg5
F
Fold increases FLuc/Rluc (normalized to Vector)
Vector
MK2EE
Vector
MK2EE
Fold Increases FLuc/RLuc (normalized to Vector NS)
Fold increases FLuc/Rluc (normalized to MK2EE NS)
NS
shNDP52
shOPTN
shp62
E
NS
Zoom
shNDP52-1
Zoom
Vector
MK2EE
Hedls puncta/cell
NS
shNDP52
shOPTN
shp62
Hairpin

Figure 7

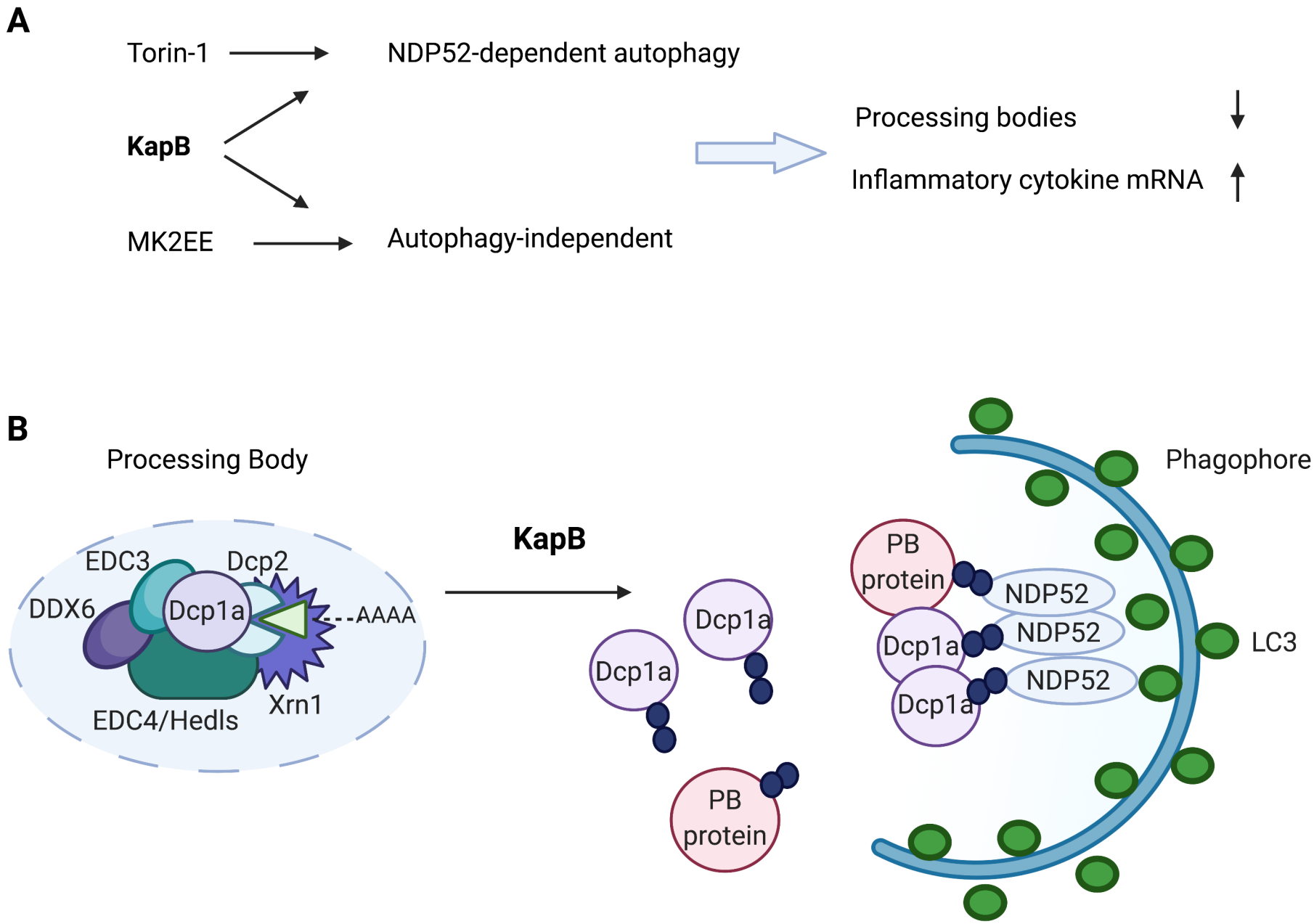
A
Torin-1
NDP52-dependent autophagy
KapB
MK2EE
Autophagy-independent
Processing bodies
Inflammatory cytokine mRNA
B
Processing Body
EDC3
Dcp2
DDX6
Dcp1a
AAAA
Xrn1
EDC4/Hedls
KapB
Dcp1a
Dcp1a
PB protein
Phagophore
PB protein
NDP52
Dcp1a
NDP52
Dcp1a
NDP52
LC3

Figure S1

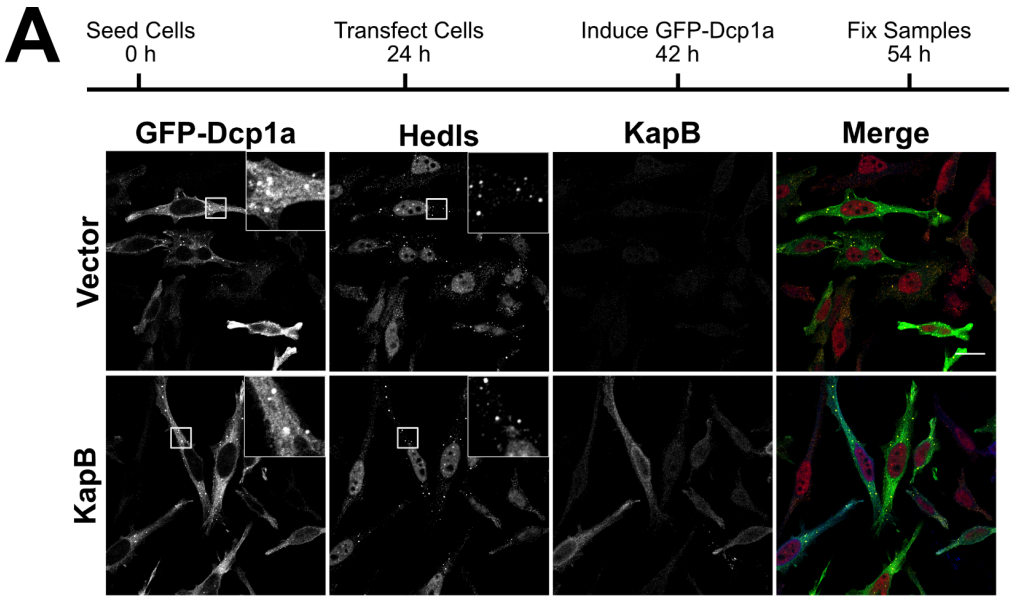
A
Seed Cells
0 h
Transfect Cells
24 h
Induce GFP-Dcp1a
42 h
Fix Samples
54 h
GFP-Dcp1a
Hedls
KapB
Merge
Vector
KapB

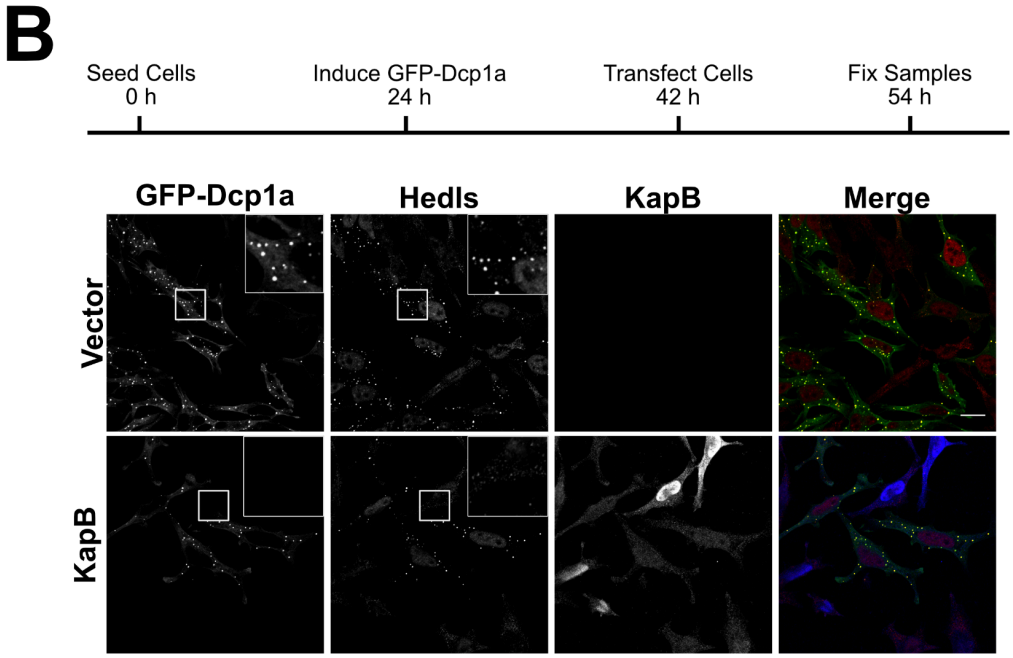
B
Seed Cells
0 h
Induce GFP-Dcp1a
24 h
Transfect Cells
42 h
Fix Samples
54 h
GFP-Dcp1a
Hedls
KapB
Merge
Vector
KapB

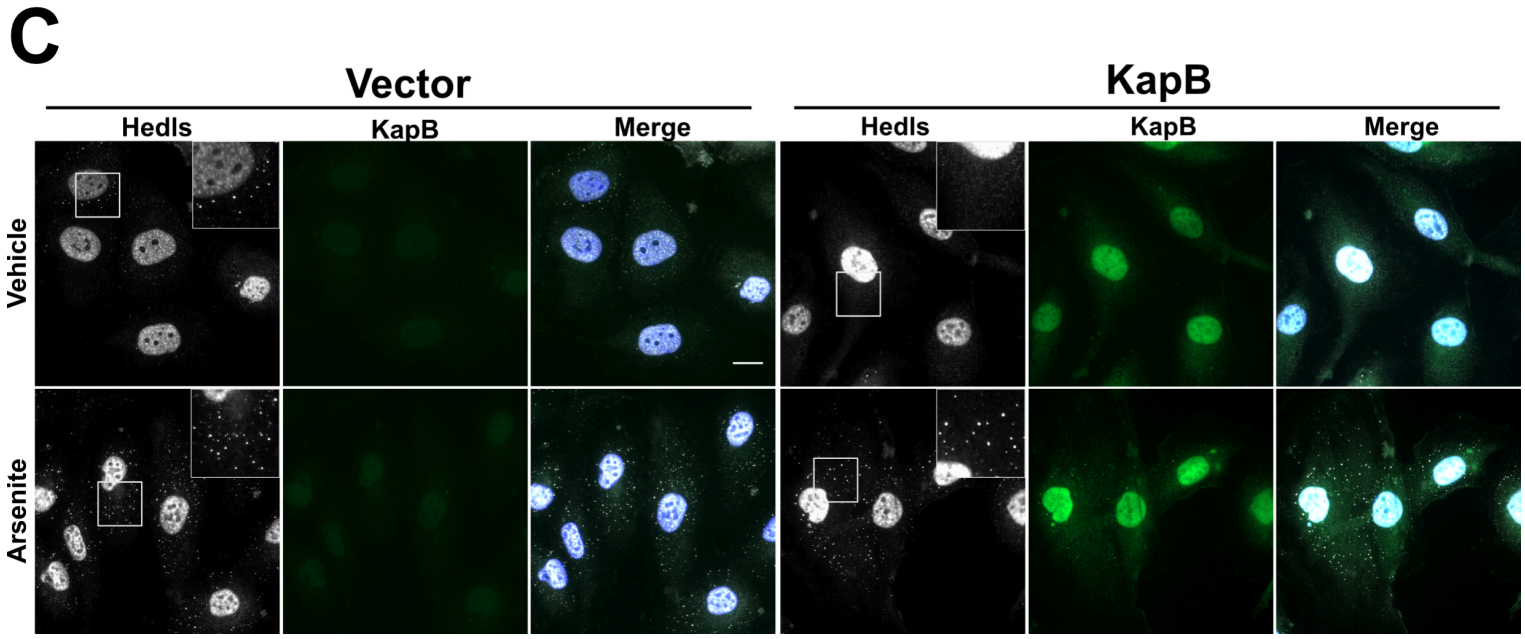
C
Vector
KapB
Hedls
KapB
Merge
Hedls
KapB
Merge
Vehicle
Arsenite

Figure S2

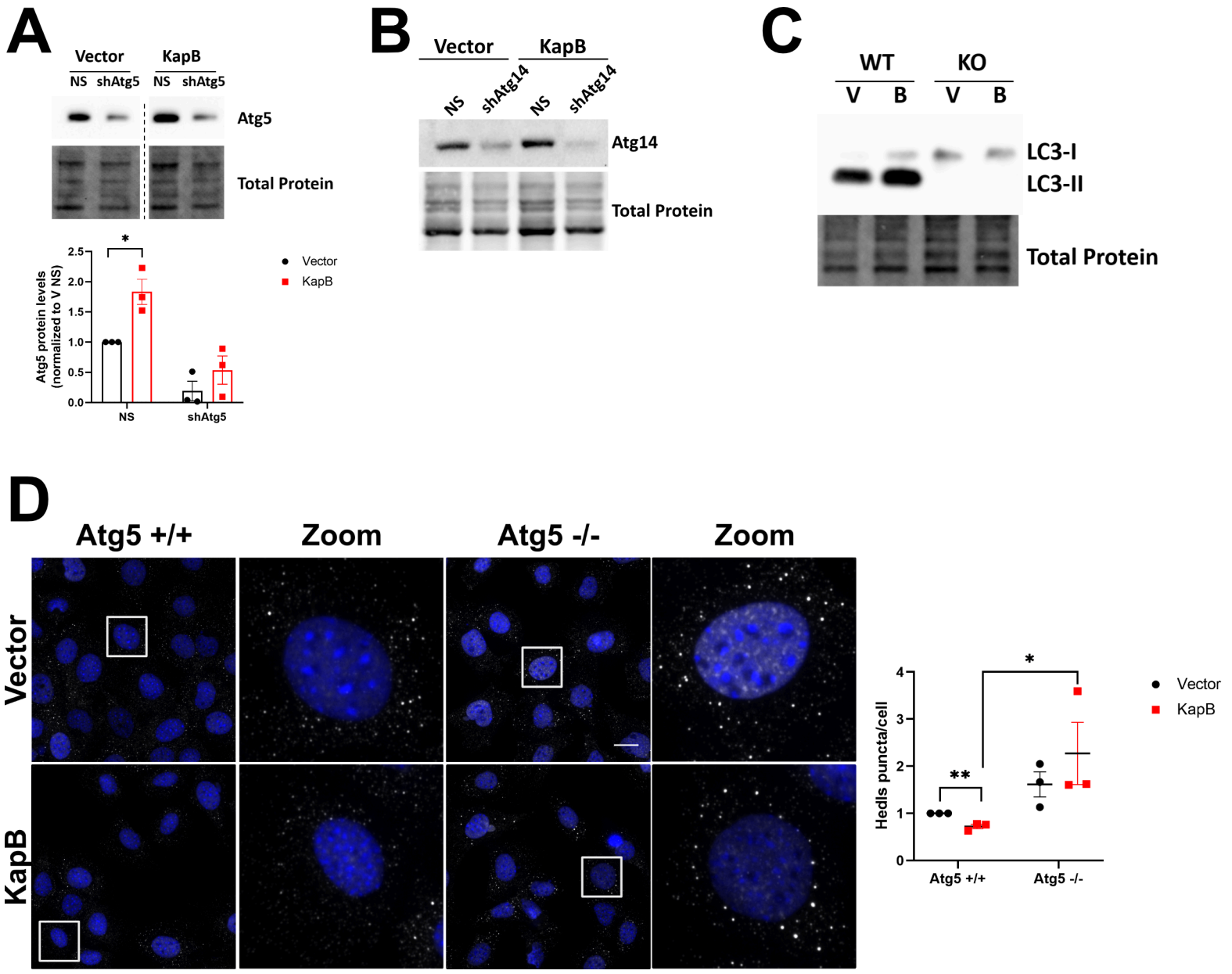
A
Vector
KapB
NS
shAtg5
NS
shAtg5
Atg5
Total Protein
*
Atg5 protein levels (normalized to V NS)
2.5
2.0
1.5
1.0
0.5
0.0
NS
shAtg5
Vector
KapB
B
Vector
KapB
NS
shAtg14
NS
shAtg14
Atg14
Total Protein
C
WT
KO
V
B
V
B
LC3-I
LC3-II
Total Protein
D
Atg5 +/+
Zoom
Atg5 -/-
Zoom
Vector
KapB
*
**
Hedls puncta/cell
4
3
2
1
0
Atg5 +/+
Atg5 -/-
Vector
KapB

Figure S3

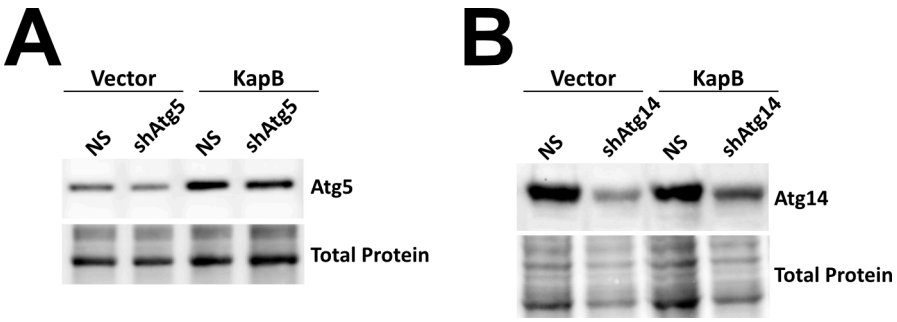
A
Vector
KapB
NS
shAtg5
NS
shAtg5
Atg5
Total Protein
B
Vector
KapB
NS
shAtg14
NS
shAtg14
Atg14
Total Protein

Figure S4

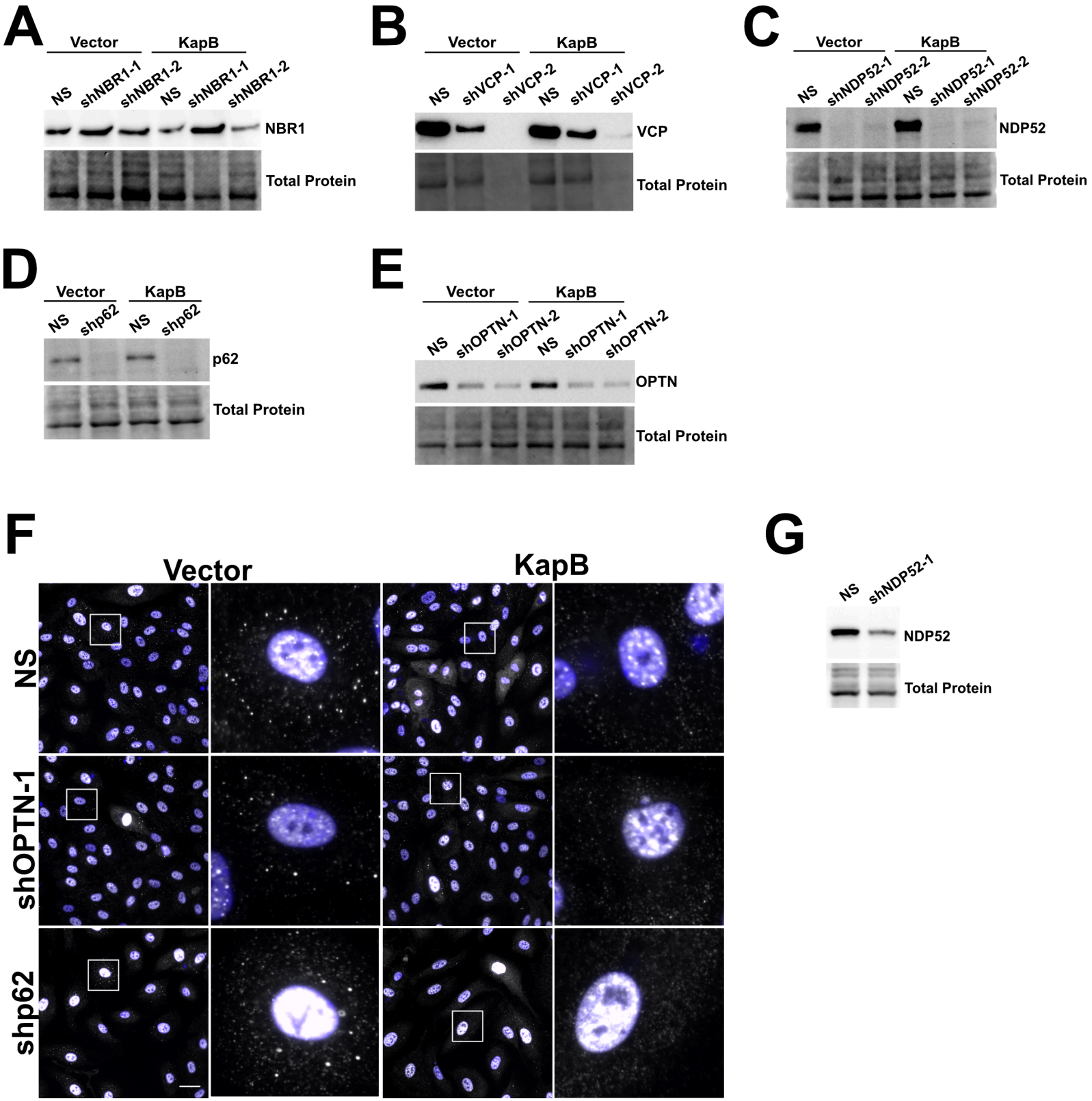
A
Vector
KapB
NS
shNBR1-1
shNBR1-2
NS
shNBR1-1
shNBR1-2
NBR1
Total Protein
B
Vector
KapB
NS
shVCP-1
shVCP-2
NS
shVCP-1
shVCP-2
VCP
Total Protein
C
Vector
KapB
NS
shNDP52-1
shNDP52-2
NS
shNDP52-1
shNDP52-2
NDP52
Total Protein
D
Vector
KapB
NS
shp62
NS
shp62
p62
Total Protein
E
Vector
KapB
NS
shOPTN-1
shOPTN-2
NS
shOPTN-1
shOPTN-2
OPTN
Total Protein
F
Vector
KapB
NS
shOPTN-1
shp62
G
NS
shNDP52-1
NDP52
Total Protein

Figure S5

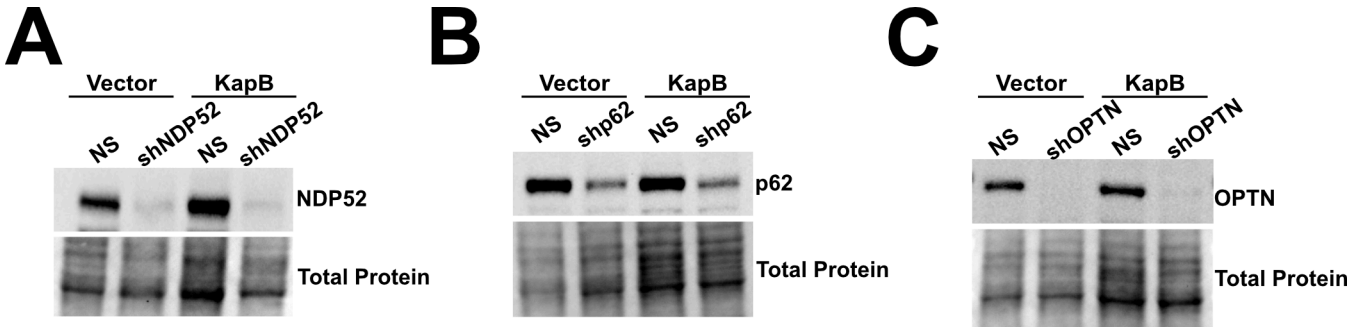
A
Vector
KapB
NS
shNDP52
NS
shNDP52
NDP52
Total Protein
B
Vector
KapB
NS
shp62
NS
shp62
p62
Total Protein
C
Vector
KapB
NS
shOPTN
NS
shOPTN
OPTN
Total Protein

Figure S6

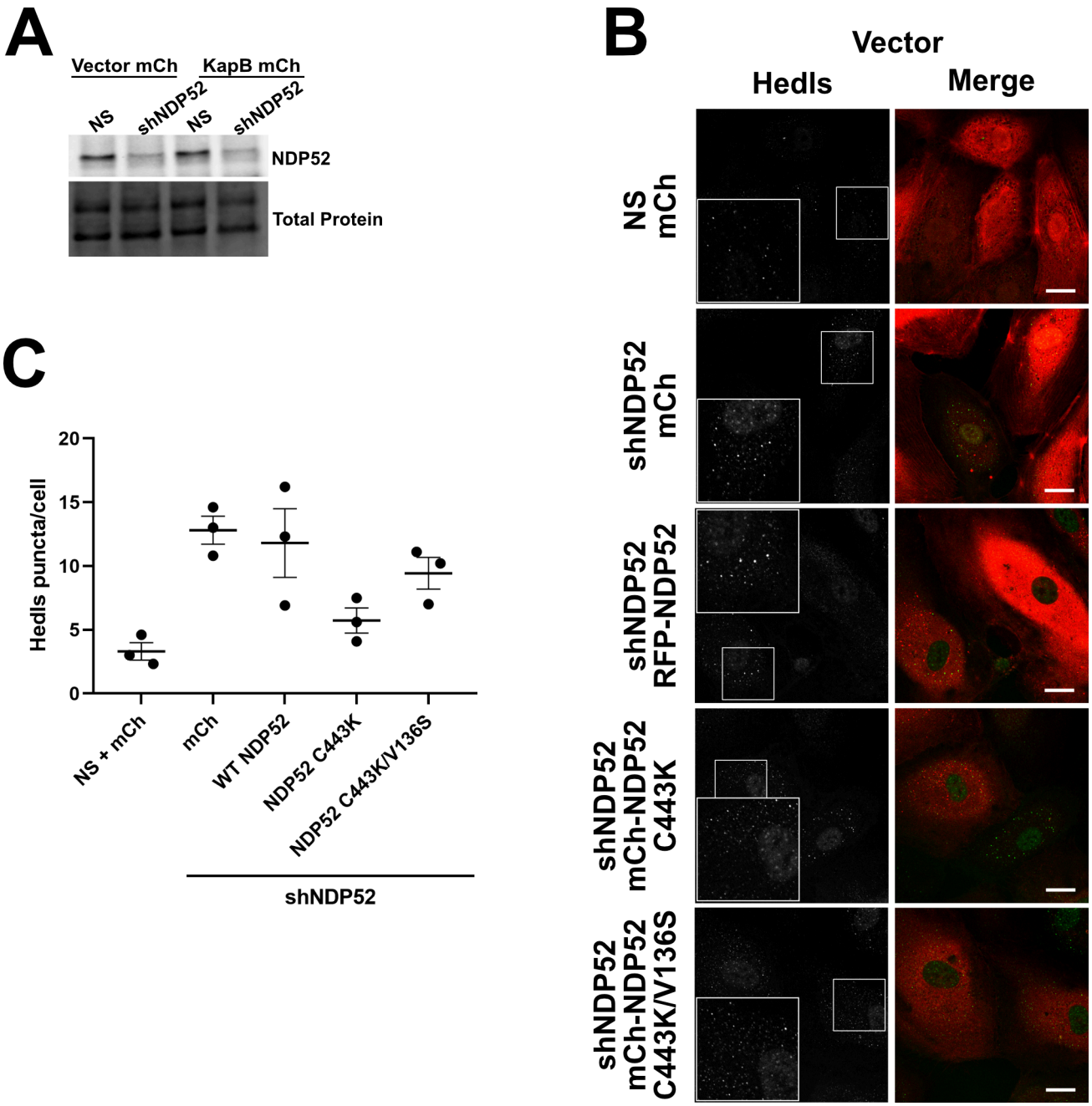
A
Vector mCh
KapB mCh
NS
shNDP52
NS
shNDP52
NDP52
Total Protein
B
Vector
HedIs
Merge
NS mCh
shNDP52 mCh
shNDP52 RFP-NDP52
shNDP52 mCh-NDP52 C443K
shNDP52 mCh-NDP52 C443K/V136S
C
HedIs puncta/cell
20
15
10
5
0
NS + mCh
mCh
WT NDP52
NDP52 C443K
NDP52 C443K/V136S
shNDP52

Figure S7

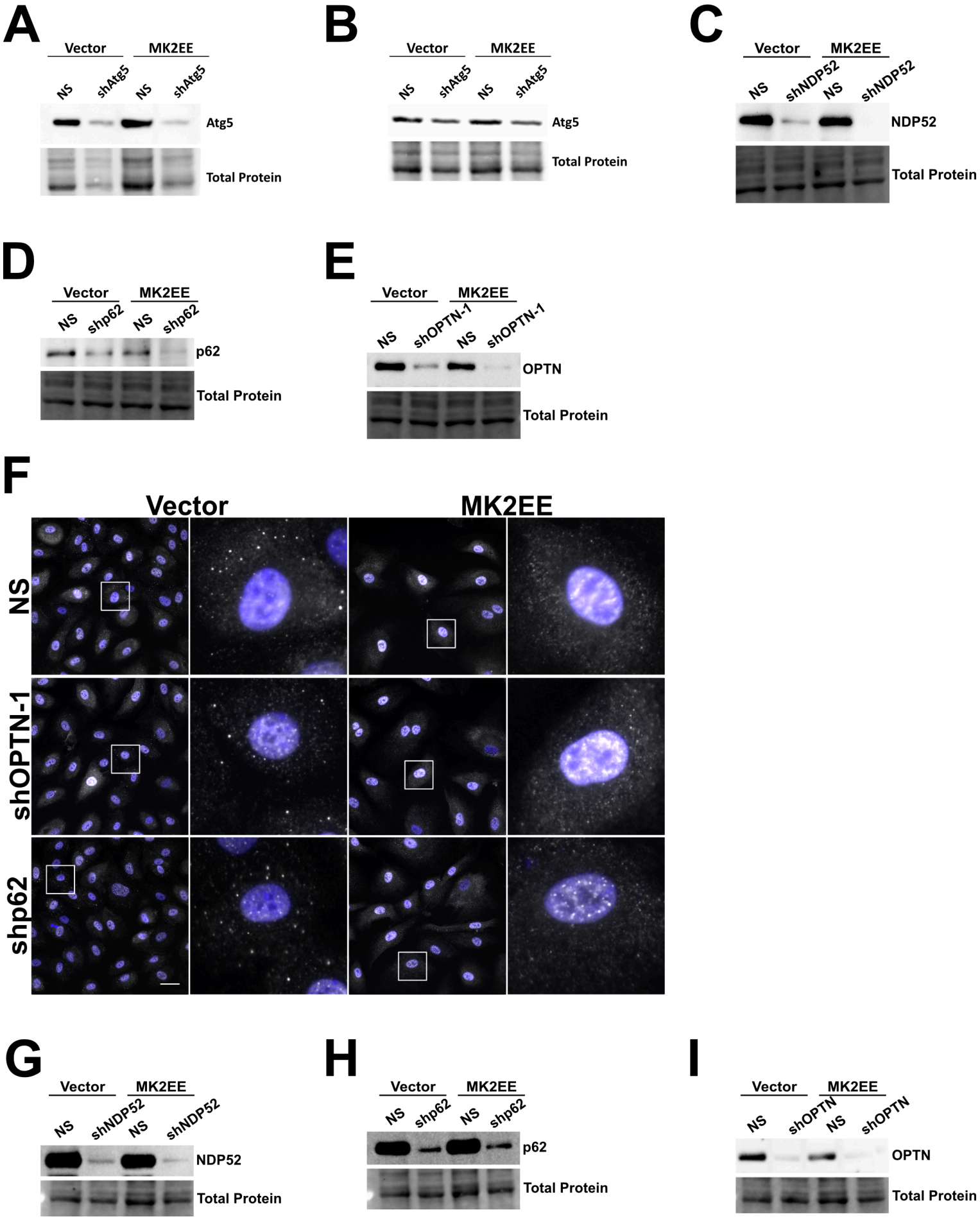
A
Vector
MK2EE
NS
shAtg5
NS
shAtg5
Atg5
Total Protein
B
Vector
MK2EE
NS
shAtg5
NS
shAtg5
Atg5
Total Protein
C
Vector
MK2EE
NS
shNDP52
NS
shNDP52
NDP52
Total Protein
D
Vector
MK2EE
NS
shp62
NS
shp62
p62
Total Protein
E
Vector
MK2EE
NS
shOPTN-1
NS
shOPTN-1
OPTN
Total Protein
F
Vector
MK2EE
NS
shOPTN-1
shp62
G
Vector
MK2EE
NS
shNDP52
NS
shNDP52
NDP52
Total Protein
H
Vector
MK2EE
NS
shp62
NS
shp62
p62
Total Protein
I
Vector
MK2EE
NS
shOPTN
NS
shOPTN
OPTN
Total Protein